Constraining the composition and thermal state of Mars from inversion of geophysical data

A. Khan[1,2] and J. A. D. Connolly[3]

Received 24 August 2007; revised 9 January 2008; accepted 19 February 2008; published 9 July 2008.

[1] We invert the most recent determinations of Martian second degree tidal Love number, tidal dissipation factor, mean density and moment of inertia for mantle composition and thermal state using a stochastic sampling algorithm. We employ Gibbs energy minimization to compute the stable mineralogy of the Martian mantle in the model system CaO-FeO-MgO-Al_2O_3-SiO_2. This procedure yields density and *P* and *S*-wave velocities in the mantle as a function of depth and temperature and permits direct inversion for composition and thermal state. We find a Martian mantle composition resembling the model composition based on geochemical analyses of Martian meteorites. A prominent discontinuity in all physical properties occurs at ~1100 km depth, marking the onset of the mantle transition zone and coincides with the olivine → wadsleyite + ringwoodite phase transition. A smaller discontinuity in the upper mantle related to the orthopyroxene → C2/c-pyroxene + garnet is also apparent. A lower mantle discontinuity is not observed, as pressure and temperature conditions at the core mantle boundary (~20 GPa, ~1800°C) are insufficient to stabilize perovskite and magnesiowüstite. The most probable core radius is ~1680 km; core state and composition are most consistent with a liquid metallic core and a density of ~6.7 g/cm^3. This implies a high S content (>20 wt%), assuming that S is the major alloying element. The most probable bulk Fe/Si ratio is ~1.2, indicating that Mars most probably accreted from material with a nonchondritic (CI) Fe/Si ratio, such as the ordinary chondrites (L and LL), which also have oxygen isotopic ratios matching those in Martian meteorites.

Citation: Khan, A., and J. A. D. Connolly (2008), Constraining the composition and thermal state of Mars from inversion of geophysical data, *J. Geophys. Res.*, *113*, E07003, doi:10.1029/2007JE002996.

1. Introduction

[2] The internal composition of the terrestrial planets provides an important constraint on the origin and evolution of our solar system. Mars is smaller than the Earth and has a lower uncompressed density, signaling that it is compositionally distinct from the Earth, and that it may therefore have accreted from a different population of planetesimals than the Earth [e.g., *Taylor*, 1999].

[3] Given the dearth of geophysical data bearing directly on the Martian interior, little was known about the internal structure of Mars prior to Mars Pathfinder mission. Mars Pathfinder and more recent missions aimed at understanding surface processes on Mars have changed this situation. In particular, measurement of the Martian moment of inertia (MOI), a function of the planetary density distribution, has provided some constraints on structure and composition of Mars. The polar MOI (the MOI about the rotation axis) was determined to high precision from an analysis of Mars Global Surveyor (MGS) tracking data as well as Mars Pathfinder and Viking Lander range and Doppler data [*Folkner et al.*, 1997; *Yoder et al.*, 2003]. In addition, gravity and topography data from MGS have been used to place constraints on the global average crustal thickness of Mars [*Wieczorek and Zuber*, 2004; *Neumann et al.*, 2004].

[4] Estimates for the Martian mantle composition derive from geochemical studies [*Dreibus and Wänke*, 1985; *Treiman*, 1986] of a set of basaltic achondrite meteorites, collectively designated the SNC's (Shergotty, Nakhla, and Chassigny), that are thought to have originated from Mars [*McSween*, 1994]. *Dreibus and Wänke* found the Martian mantle to contain about 17 wt% FeO compared to the Earth's upper mantle budget of ~8 wt% [*McDonough and Sun*, 1995]. This implied a Martian mantle Mg (molar Mg/Mg + Fe) of 0.75, in comparison to the magnesian-rich terrestrial upper mantle value of ~0.9. The observed depletion of the SNC's in chalcolphile elements moreover suggested a substantial core component of S.

[5] Further information on the internal constitution and evolution of Mars is also provided by the state of the core, as the amount of any alloying element, notably S, not only determines its physical state, but also provides information on the areotherm. Recent analysis of the solar tidal defor-

[1]Niels Bohr Institute, University of Copenhagen, Copenhagen, Denmark.
[2]On leave at Institute of Geophysics, Swiss Federal Institute of Technology, Zurich, Switzerland.
[3]Earth Sciences Department, Swiss Federal Institute of Technology, Zurich, Switzerland.

0148-0227/08/2007JE002996

mation of Mars using MGS radio tracking data, resulted in a large value of the second degree tidal Love number ($\sim$0.15) implying the presence of a fluid core or at least of an outer liquid core [*Yoder et al.*, 2003]. Additional refinements on core state have come from recent experimental studies of phase relations in the Fe-S and (Fe,Ni)-S systems at temperatures and pressures equivalent of the Martian center (2200 K and 40 GPa). These point to an entirely liquid core at present [*Stewart et al.*, 2007], in line with evidence provided by thermal history models [*Breuer and Spohn*, 2003; *Williams and Nimmo*, 2004].

[6] The *Dreibus and Wänke* [1985] model composition of Mars has formed the basis for a number of studies that have tried to estimate the geophysical consequences of assuming that the composition of the SNC's is not only directly related to the mantle composition, but also globally representative of Mars. The numerical approach adopted by e.g., *Longhi et al.* [1992], *Sohl and Spohn* [1997], *Sohl et al.* [2005], *Verhoeven et al.* [2005], and *Zharkov and Gudkova* [2005] involves assuming a model composition, areotherm and mantle mineralogy from which physical properties are calculated using equation of state modeling, while *Kuskov and Panferov* [1993] employ a thermodynamic model to construct phase relationships in the FeO-MgO-SiO_2 (FMS) chemical system and physical properties of the Martian upper mantle. The study by *Bertka and Fei* [1997] represents the experimental approach, where high-pressure experiments are performed on the model composition of *Dreibus and Wänke* [1985] to determine its mineralogy, which is subsequently turned into a density profile. *Lodders and Fegley* [1997], *Sanloup et al.* [1999], and *Burbine and O'Brien* [2004] are representative of yet other modeling avenues, where the bulk composition is unknown and it is attempted to build Mars from different chondrite groups, subject to geochemical constraints such as the SNC oxygen isotopic ratio. Some of these studies will be considered in more detail in the following section.

[7] There are several caveats with these approach. First, the studies by *Longhi et al.* [1992], *Sohl and Spohn* [1997], and *Bertka and Fei* [1997, 1998a], for example, are forward models rather than inversions, and provide little information on the range of physical models that are consistent with the geophysical parameters for Mars. Second, they neglect the importance of phase equilibria. The latter are not only important because of the pressure induced changes in the relative proportions of the different minerals, but also because the different minerals have different physical properties. Third, regardless of their provenance the SNC meteorites that form the basis for the *Dreibus and Wänke* [1985] composition are products of partial melting and therefore, at best, provide only indirect evidence for the Martian mantle composition.

[8] In view of these limitations we reexamine some of the notions which have come from assuming a SNC model composition for the Martian mantle, by jointly inverting the most recent set of geophysical data for Martian mantle and core composition as well as thermal state. These include mean MOI (I), mean density ($\bar{\rho}$), second degree tidal Love number (k_2), tidal dissipation factor (Q), and mean radius (R). Issues that we wish to reevaluate include: extent of mantle FeO enrichment; presence of a perovskite-rich layer at the base of the mantle; core size, state and composition; and bulk Fe/Si ratio.

[9] The method that we use is based on a unified description of the elasticity and phase equilibria of multicomponent, multiphase assemblages from which mineralogical and seismic wave velocity models as functions of pressure (depth) and temperature are constructed [*Connolly and Kerrick*, 2002; *Stixrude and Lithgow-Bertelloni*, 2005]. By virtue of a set of criteria underlying our approach, its formulation is experimentally and theoretically well founded, leading to the estimation of physical properties (e.g., seismic wave speeds) that depend only on the specified temperature, pressure and composition. The criteria are, isotropy of the mineral aggregate, homogeneity of bulk composition, absence of elastic wave dispersion, subsolidus conditions (no partial melt), and thermodynamic equilibrium. The advantage of our method is not only that a direct inversion for composition and temperature is rendered possible, but also that a natural integration of the different geophysical data in the inversion is achieved. By integrating different geophysical data, our method also provides a means of putting tighter constraints on the internal constitution and structure of Mars than previously possible. The generality of the method employed here makes it easily extendable to include other sets of geophysical, and even geochemical data.

[10] The methodology of our inversion scheme is described in detail in our previous studies [*Khan et al.*, 2006a, 2006b, 2006c]. Other extraterrestrial applications along present lines include those of *Kuskov et al.* [2002] and *Kuskov and Kronrod* [2001, 2005]. The following sections include reviews of some earlier Martian studies followed by a brief description of the geophysical data, after which we describe modeling aspects and finally present and discuss results. For recent reviews of Mars, the reader is referred to *Stevenson* [2001], *Zuber* [2001], and *Solomon et al.* [2005].

2. Previous Investigations of Mars Internal Structure

[11] Our knowledge of the composition of the Martian mantle comes from geochemical studies of the SNC meteorites, a set of basaltic achondrite meteorites that are produced by mantle melting [*Dreibus and Wänke*, 1985] (hereafter referred to as DW). DW aimed at inferring the bulk composition of Mars by estimating the ratios of major chalcophile, siderophile and volatile elements in the SNC's, assuming all refractory elements present in CI chondritic ratios, as well as a bulk planet composition with a CI chondrite Fe/Si ratio. This model Martian composition will hereinafter be referred to as DW-SNC.

[12] *Longhi et al.* [1992] converted the DW-SNC composition to a pressure-dependent mineralogy and used the estimated density model to calculate its MOI (from hereon MOI refers to the dimensionless value, i.e., normalized by MR^2, where M and R are planetary mass and radius, respectively) and compare it with observation. Their model consisted of a 100 km thick crust (with a density of 2.7 g/cm^3), a mantle divided into two parts, and a core. The upper mantle extended down to the olivine $\rightarrow$ wadsleyite + ringwoodite transition (900–1100 km depth, 12–14 GPa)

and the lower mantle made up the rest. As on Earth, the upper mantle was found to be dominated by olivine, with orthopyroxene being the next most abundant mineral. Transition zone mineralogy was made up principally of spinel and majorite. Lower mantle mineralogy depended on the size of the core, and in turn on its composition. The preferred core composition, containing 14.5 wt% S with a radius of ~1695 km, predicted the presence of a perovskite layer above the core mantle boundary (CMB, at 23.5 GPa). Using melting relations for Fe and FeS measured over the pressure range appropriate for the Martian mantle, they estimated that a completely solid Martian core, of the preferred composition above, would be 2200 ± 250 K, while the minimum temperature for a liquid core would be 2400 ± 250 K. The corresponding upper bound on temperature at the CMB was estimated to be 1800 K ± 350 K and 2000 ± 350 K, respectively. The mean MOI of the final model was 0.353 and agreed with the geochemical constraint of a global Fe/Si carbonaceous CI chondrite ratio of 1.71.

[13] *Kuskov and Panferov* [1993] constructed thermodynamic models for the structure of Mars upper mantle on the basis of the FeO-MgO-SiO_2 (FMS) chemical system using Gibbs free energy minimization, and as such is closely related to the present study. The chemical composition investigated consisted of 40 mol% SiO2, Fe#(=Fe/(Fe + Mg)) of 0.2–0.25, and an olivine/pyroxene (α/Px) molar ratio of 1. The pressure distribution within the planet is also crucially dependent on core composition, which in the model of Kuskov and Panferov was made of Fe-20 wt% S. For an assumed MOI of 0.365, and the above FMS comp, a core radius and CMB pressure of 1386 km and 24.8 Gpa, respectively, were estimated. The unknown areotherm was modeled using a number of gradients, which were 2.4 K/km (0–500 km depth), 0.6 K/km (500–1000 km depth) and 0.2 K/km at deeper depths. Phase relationships were calculated in the pressure range 10–15 GPa (820–1250 km depth) and for the composition with Fe# = 0.2 the following phases and transformations were found: $\alpha + \mathrm{Px} \xrightarrow{1050} \alpha + \gamma + \mathrm{Px} \xrightarrow{1160} \beta + \gamma + \mathrm{Px} \xrightarrow{1180} \gamma + \mathrm{Px}$, where numbers indicate phase transition depths in km, and β and γ are short for β- and γ-spinel, respectively. The derived seismic wave velocity profiles (see Figure 7) showed no sharp discontinuity, leading the authors to suggest that the Martian mantle lacks the terrestrial analogue of the prominent 410 km upper mantle/transition zone boundary which is due to the transformation of olivine to wadsleyite. The authors do, however, note that their picture of the Martian mantle might possibly be incomplete, as transitions due to Px-garnet are not considered.

[14] *Sohl and Spohn* [1997] analyzed two end-member scenarios for the internal structure of Mars. One model was made to satisfy the most probable maximum value of the MOI of 0.366 (model A), whereas the other model (model B) had to satisfy the geochemical constraint of a bulk CI chondritic Fe/Si ratio of 1.71. Their models, based on DW-SNC, were parameterized as consisting of a basaltic crust 100 to 250 km in thickness, upper and lower mantle separated by the α-olivine to β-spinel transition, which was further subdivided into β-spinel and very thin γ-spinel layers, and a metallic core. Solving an isothermal Birch-Murnaghan type equation of state together with a set of fundamental differential equations governing mechanical and thermal structure, enabled them to derive the physical properties of the Martian interior. For Model A, satisfying the geophysical constraint, an Fe/Si ratio of 1.35 was determined, whereas for geochemical model B, a MOI of 0.357 was estimated. In addition, the calculations suggested a Fe-Ni-FeS core (radius ~1600 km), with central temperatures in the range 2000–2200 K. Also, mantle pressures were found not to be sufficiently high for the spinel to perovskite transition to occur.

[15] *Zharkov and Gudkova* [2005], in a recent analysis, investigate a range of Martian interior structure models and compare these to the recent data determinations of k_2 and MOI by *Yoder et al.* [2003], including a detailed analysis of anelastic contributions to k_2. Their analysis is based on a four-layer model, divided into near-surface crustal layer, crust, mantle and core. The composition of the crust is derived from four SNC meteorites and its mineralogy and seismic properties are determined thermodynamically [*Babeiko and Zharkov*, 1997]. Crustal thickness is taken to be either 50 or 100 km thick. Mantle mineralogy and physical properties are based on the experimental study of *Bertka and Fei* [1997] (to be discussed below) and equation of state modeling following the approach of *Duffy and Anderson* [1989]. The variable mantle parameter is Fe content, with Mg# varying between 0.75 and 0.82. In the planetary accretion model of *Zharkov* [1996], the Martian core is believed to contain H in addition to S, as the solution of H in Fe becomes favorable at increased gas pressure. On the basis of the reactions $\mathrm{Fe} + \mathrm{H_2O} \rightarrow \mathrm{FeO} + \mathrm{H_2}$ and $\mathrm{Fe} + (x/2)\mathrm{H_2} \rightarrow \mathrm{FeH}_x$, and a H_2O budget of 7.3 wt% in CI chondrites and assuming that all of this reacts and moreover, that all H_2 produced is incorporated into the core, Zharkov determines a maximum core H abundance of 0.16 wt% of the planet's mass. Core properties for various compositions (14–36 wt% S, 0–70 mol% H) were determined using finite strain theory. The authors find that models satisfying k_2 and Q have mantle Mg#'s in the range 0.78–0.82, liquid cores with radii in the range 1625–1816 km, and compositions containing 14 wt% S and 50 mol% H. The bulk Fe/Si ratio for the preferred model is close to chondritic (CI). Estimated MOI for these models were between 0.3633–0.3674.

[16] In an experimental investigation, *Bertka and Fei* [1997] subjected DW-SNC to high pressures (up to 23.5 GPa) along a high temperature model thermal profile (CMB temperatures around 2000 K) to determine the mineralogy of the Martian interior, which was subsequently turned into a resulting density profile [*Bertka and Fei*, 1998a]. As in the study of Longhi et al., Bertka and Fei found an upper mantle consisting of olivine + pyroxene and garnet (up to 9 GPa), a transition zone dominated by an assemblage of γ-spinel and majorite (up to 17 GPa) and a lower mantle made up of Mg-Fe silicate-perovskite, magnesiowüstite and majorite, while calcium-perovskite was not found to be stable. The presence of a perovskite layer a few hundred km thick above the CMB depended, as in other studies, strongly on core size and thus its composition as well as temperature in the deep mantle. This study concluded that the DW-SNC, with a Fe-14 wt% S core (radius ~1300 km, assuming crustal density and thickness in the ranges 2.7 to 3 g/cm^3 and 25 to 150 km, respectively), could not be made to fit the MOI if a bulk CI chondritic Fe/Si ratio was to be maintained.

[17] Another means at inferring bulk composition, physical structure and core size, is the avenue taken by *Sanloup et al.* [1999], who consider the aforementioned attempts as relying too heavily on compositional constraints implied by the SNC's, such as the meteorites being fractionated rocks and the refractory elements occurring in CI chondritic abundance ratios. Instead, *Sanloup et al.* [1999] argue for the oxygen isotopic composition of the SNC's to be used as constraint and to model Mars as a mixture of chondritic material. This stems from the recognition, as they note, that the abundance and isotopic composition of oxygen in meteorites is a prominent source for the classification of the latter. They go on to hypothesize that Mars is made up of a mixture of enstatite (EH) and ordinary (H) chondrites, given that Mars lies in-between the Earth, with an oxygen isotopic composition akin to enstatite chondrites, and the asteroid belt, the potential source of ordinary chondrites, while the oxygen isotopic composition of the SNC's has been found to be intermediate between the two chondrite types [*Clayton et al.*, 1991]. Given two model compositions then, in proportions EH45:H55 (model 1) and EH70:H30 (model 2), in addition to a physical model (3rd-order isothermal Birch-Murnaghan equation of state) and a thermal profile (adiabatic gradients in the mantle and core), resulted in CMB temperatures around 1850 K, core radii, MOI factors, Mg#'s and Mg/Si ratios of 1710 ± 5 km, 0.361 ± 0.002, 0.72, 1.17 (model 1) and 1865 ± 5 km, 0.361 ± 0.002, 0.8, 0.98 (model 2), respectively.

[18] The study by *Burbine and O'Brien* [2004] is along the lines of *Sanloup et al.* [1999], in that they try to match Mars' oxygen isotopic compositions using known chondritic material, but also add a bulk chemical constraint on FeO content (14.4 ± 1.4 wt%). Over 225 million possible combinations of different chondritic meteorites are tried in order to find the best matches. The analysis showed that H and LL chondrites could make up 80% and L chondrites 75% of matching combinations, respectively, resulting in an average Fe/Si ratio of 1.51 ± 0.17. These results agree with those from *Lodders and Fegley* [1997], who, in a similar combinatorial analysis, found possible building blocks to be made out of 85% H, 11% CV, and 4% CI chondrites.

3. Geophysical Data

[19] The geophysical data most recently made available which can be used to provide constraints on the internal constitution and structure of Mars are its mean density, its mean MOI, second degree tidal Love number, being a measure of the rigidity of Mars, tidal dissipation factor, accounting for the tidal energy that is dissipated within the solid body during a tidal cycle of Mars and finally, its mean radius. The analysis by *Yoder et al.* [2003] has provided the most accurate determination of the polar MOI (the MOI about the rotation axis) of 0.365 ± 0.0012, which is slightly lower than the value determined by *Folkner et al.* [1997] of 0.3662 ± 0.0017. However, rather than use the polar MOI to construct spherically symmetric models one should employ the mean MOI, which has recently been determined by *Sohl et al.* [2005] to be 0.3635 ± 0.0012, based on the polar MOI of Yoder et al., Mars' gravitational oblateness and small contributions arising from Tharsis. For the mean density ($\bar{\rho}$) we use the value by *Esposito et al.* [1992] of 3.935 ± 0.0004 g/cm^3.

Table 1. Summary of Areophysical Data Parameters d_{obs} and Their Uncertainties σ Used in the Inversion

Data Parameter	$d_{obs} \pm \sigma$
$\bar{\rho}$	3.935 ± 0.0004 g/cm^3
I/MR^2	0.3635 ± 0.0012
k_2	0.145 ± 0.017
Q	92 ± 11
R	3389.5 km

[20] Analysis of the solar tidal deformation of Mars by Yoder et al. resulted in a value for k_2 of 0.145 ± 0.017. This is good agreement with the most recent determination of 0.148 ± 0.009 by *Konopliv et al.* [2006] using 6 years of MGS and 3 years of Mars Odyssey tracking data. This number is the purely elastic value, i.e., contributions from anelastic effects have been removed. For a detailed discussion of anelastic contributions to k_2 see, e.g., *Zharkov and Gudkova* [2005]. This value differs considerably from that determined by *Smith et al.* [2003]. They found $k_2 = 0.055 \pm 0.008$, implying that the Martian core has solidified, in stark contrast to the conclusions drawn by *Yoder et al.* of a presently liquid Martian core. That $k_2 > 0.1$ implies a liquid, and $k_2 < 0.1$ a solid core, had already been deduced by *Lognonné and Mosser* [1993] and *Zharkov and Gudkova* [1997]. In an independent recent determination of k_2, *Bills et al.* [2005] obtained $k_2 = 0.163 \pm 0.056$, in general agreement with Yoder et al. The intricacies involved in determining k_2 from MGS data are discussed by *Smith et al.* [2003] and *Bills et al.* [2005].

[21] Estimates of Mars' global tidal dissipation Q (also known as tidal quality factor) include an earlier determination, obtained from the orbital acceleration of Phobos, of 100 ± 50 [*Yoder*, 1982], while *Bills et al.* [2005] obtained a Q of 85.58 ± 0.37, which is in overall agreement with the value derived by *Yoder et al.* [2003] of 92 ± 11. A recent determination by *Lainey et al.* [2007] of the ephmerides of the Martian moons resulted in a Q of 79.91 ± 0.69. We use the value derived by *Yoder et al.* [2003] as the quoted error estimate by *Bills et al.* [2005] does not consider, among other things, the uncertainty in the elastic Love number and other contributing factors.

[22] The geophysical data employed here are summarized in Table 1.

4. Method of Analysis

4.1. Construction and Solution of the Forward Problem

[23] We assume a spherically symmetric model and represent Mars by three concentric shells of unspecified thickness that correspond to crust, mantle and core. Crust and mantle are delineated by the model parameters thickness d, composition c and temperature T, whereas the core is parameterized by radius r_c, density ρ_c, shear and pressure wave velocities V_S^c, V_P^c, respectively. To determine the mineralogical structure and physical properties it is also necessary to specify the pressure profile in addition to composition and temperature. For this purpose the load is integrated from the surface and down to the CMB.

Table 2. Phase Notation, Formulae and Solution Model Sources[a]

Symbol	Phase	Formula	Source
An	anorthite	$Ca_2Al_2Si_2O_8$	
Ca-pv	calcium perovskite	$CaSiO_3$	
Cpx	clinopyroxene	$Ca_{2y}Mg_{4-2x-2y}Fe_{2x}Si_4O_{12}$	[1]
Gt	garnet	$Fe_{3x}Ca_{3y}Mg_{3(1-x+y+z/3)}Al_{2-2z}Si_{3+z}O_{12}$, $x + y + 4z/3 \leq 1$	[1]
Ol	olivine	$[Mg_xFe_{1-x}]_2SiO_4$	[1]
Opx	orthopyroxene	$[Mg_xFe_{1-x}]_{4-2y}Al_{4(1-y)}Si_4O_{12}$	[1]
Sp	spinel	$Mg_xFe_{1-x}Al_2O_3$	[1]
C2/c	pyroxene	$[Mg_xFe_{1-x}]_4Si_4O_{12}$	[1]
Aki	akimotoite	$[Mg_xFe_{1-x}]_{1-y}Al_{2y}Si_{1-y}O_3$	[2]
Pv	perovskite	$[Mg_xFe_{1-x}]_{1-y}Al_{2y}Si_{1-y}O_3$	[2]
Ring	ringwoodite	$[Mg_xFe_{1-x}]_2SiO_4$	[1]
Wad	wadsleyite	$[Mg_xFe_{1-x}]_2SiO_4$	[1]
Wus	magnesiowüstite	$Mg_xFe_{1-x}O$	[2]

[a]Unless otherwise noted, the compositional variables x, y, and z may vary between zero and unity and are determined as a function of the computational variables by free-energy minimization. Thermodynamic data for pure phases and end-member compositions is from *Stixrude and Lithgow-Bertelloni* [2005] augmented for lower mantle phases as described by *Khan et al.* [2006b]. Solution model sources: [1] *Stixrude and Lithgow-Bertelloni* [2005]; [2] *Fabrichnaya* [1998].

[24] Calculating data **d** from a set of model parameters **m** using a physical law g is usually written in short form as **d** = g(**m**). More explicitly, this equation can be decomposed into

$$m_1 \xrightarrow{g_1} m_2 \begin{cases} \xrightarrow{g_2} d_1 \\ \xrightarrow{g_3} d_2 \\ \xrightarrow{g_4} \mathbf{d}_3 \end{cases}$$

where $\mathbf{m}_1$ is a model parameter vector containing the above parameters and $\mathbf{m}_2$ contains modal mineralogies and mantle physical properties (density, P and S wave velocities). The g's are forward operators, embodying the physical laws, where g_1 is the Gibbs free energy minimization routine, which calculates mineral phase proportions (modal mineralogy) and bulk physical properties. g_2, g_3, and g_4 are the forward operators calculating k_2, Q, $\bar{\rho}$ and I, respectively, which are contained in d_1, d_2, and $\mathbf{d}_3$.

4.2. Thermodynamical Modeling

[25] Martian compositions were explored within the system CaO-FeO-MgO-Al_2O_3-SiO_2; a chemical model that accounts for more than 98% of the mass of the Martian mantle of *Bertka and Fei* [1997] for the DW-SNC composition. The Martian mineralogy is assumed to be dictated by equilibrium and computed from thermodynamic data for a given model pressure, temperature and bulk composition by Gibbs energy minimization [*Connolly*, 2005]. These calculations were made taking into consideration the phases summarized in Table 2. The requisite thermodynamic properties at pressure and temperature were obtained using the equation of state proposed by *Stixrude and Bukowinski* [1990] with parameters as given by *Stixrude and Lithgow-Bertelloni* [2005]. For lower mantle conditions, the data of *Stixrude and Lithgow-Bertelloni* [2005] were augmented by the end member data for magnesiowuestite, calcium perovskite, and the ferrous and aluminous perovskite endmembers as detailed by *Khan et al.* [2006b]. The equilibrium assumption is dubious at low temperature [e.g., *Wood and Holloway*, 1984]. In recognition of this limitation, if a model required a mineralogy at a temperature below 1073 K, then the equilibrium mineralogy was calculated at 1073 K. Physical properties for the mineralogy so obtained were then computed at the temperature of interest. *Stixrude and Bukowinski*'s [1990; *Stixrude and Lithgow-Bertelloni*, 2005] equation of state provides the adiabatic bulk and shear moduli of the minerals predicted by Gibbs energy minimization as a function of pressure, temperature and composition. Bulk elastic moduli were taken as the Voigt-Reuss-Hill volumetric average of the mineral moduli under the assumption that textural anisotropy is negligible.

[26] Gibbs energy minimization predicts stable mineralogies as a function of pressure, temperature and bulk composition by simultaneously optimizing the properties of all the minerals that are considered to be potentially stable. The minerals are not considered individually, indeed they cannot be in any thermodynamic treatment, and properties such as partition coefficients are determined entirely by, and consistently with, the thermodynamic data used for the calculation. This thermodynamic data consists of semiempirical equations of state that have been independently tested and calibrated [*Stixrude and Lithgow-Bertelloni*, 2005]. Ideally, the calibration of the equations of state distills experimental data into a single coherent result that embodies the state of knowledge. The theoretical basis of the equation of state allows some confidence when the data are used at conditions beyond which it was calibrated. In the context of Mars, the range of compositions and physical conditions considered require extrapolations that are comparable to those that would be required to do similar models for the Earth. Therefore there is no reason to suspect that the thermodynamic data used here, which was developed for terrestrial studies cannot be applied to Mars.

[27] The present thermodynamic model has limitations that may have consequences for its validity to Mars. First, the model system CaO-FeO-MgO-Al_2O_3-SiO_2 precludes consideration of redox effects that might be expected to be important if native or ferric iron are present in the Martian mantle. We neglect such effects both out of necessity, in that the thermodynamic data required to model redox is lacking, and simplicity, in that we are unaware of any work that suggests that ferrous iron is not the dominant form of iron in the Martian mantle. Second, the model only accounts for the stability of minerals thought to be present

in significant quantities in the terrestrial mantle. While stishovite is not an important constituent of the terrestrial mantle it has been suggested that it may be important on Mars [*Bertka and Fei*, 1997]. Unfortunately, the thermodynamic data for stishovite provided by *Stixrude and Lithgow-Bertelloni* [2005] predicts an excessive stability field for stishovite for pyrolitic bulk compositions. Given this source of uncertainty, we have excluded stishovite from our calculations. Last, we neglect the solubility of Ca in orthopyroxene, an effect that would lead to higher modes of orthopyroxene and its C2/c polymorph relative to Ca-rich clinopyroxene.

4.3. Calculating Love Number and Tidal Dissipation

[28] A planet subjected to an external gravitational tidal potential Φ will deform and the deformation will give rise to an induced potential Φ' related to the former through

$$\Phi' = k_2 \Phi \tag{1}$$

where the constant of proportionality is the tidal potential Love number (here to second order). The amount of deformation undergone by the body depends on the internal properties, in the sense that if the bodies elastic rigidity is sufficient, it will experience little deformation with a resulting small value for k_2. Estimating Love numbers for a nonhomogeneous planet, given knowledge of its density and elastic wave velocity structure, is a well expounded problem in solid Earth geophysics and will not be reiterated here. In practice, k_2 is obtained by numerical integration using the approach of e.g. *Alterman et al.* [1959].

[29] If Mars were purely elastic there would be no internal dissipation of energy in its orbit about the Sun. However, Mars like other planetary bodies is anelastic giving rise to dissipation of energy. This is usually expressed in terms of the quality factor Q. Generally, $1/Q$ is defined as the ratio of energy dissipated to peak energy stored in the system during an orbit. In terms of equation (1), this means that for a purely elastic body with no dissipation, external and induced potentials Φ and Φ', respectively, remain aligned as there is no influence on the orbit. If dissipation is present as it would be in a viscoelastic body, the two potentials would no longer be aligned, with the deformation lagging behind the external potential. The greater the dissipation, the more Φ and Φ' will be out of phase. In order to quantify this, expressions for the average energy dissipated to that stored over one orbit as a function of parameters that depend on the internal structure of the planet, are sought. In this manner global tidal dissipation can be shown to be calculated from $Q^{-1} = Im(k_2)/Re(k_2)$, where $Re(k_2)$ is the elastic part of the second degree tidal Love number calculated above and $Im(k_2)$ is its anelastic part, which is related to the amount of energy being dissipated [e.g., *Segatz et al.*, 1988]. The theoretical derivation of the anelastic contribution to k_2 in the general case of a nonhomogeneous body is developed by, e.g., *Zschau* [1978], *Wahr and Bergen* [1986], and *Segatz et al.* [1988]. We follow our earlier approach [*Khan et al.*, 2004], which is based on the study of *Wahr and Bergen* [1986].

[30] In the case of anelasticity the elastic parameters and Love numbers become complex and frequency (ω) dependent. Evidence suggests that in the seismic frequency band Q is only weakly dependent upon frequency, as $\sim\omega^{\alpha}$, where α has been measured experimentally to be around 0.1–0.2 [*Jackson et al.*, 2002]. In addition, results by *Benjamin et al.* [2006] suggest that the dissipative process could consist of a single absorption band that extends across seismic periods out to about 20 years. Relying on recent results of *Zharkov and Gudkova* [2005], who showed that Q and elastic moduli for Mars, notably shear modulus, are only weakly dependent on frequency (Q was found to change from 92 ± 11 to 83.3 ± 9.5 and μ by <0.5% on going from a period of 12 to 5.55 h). Based on this, we assume without much loss of precision Q as well as elastic parameters to be independent of frequency.

[31] In the general case shear modulus μ is given by (assuming that loss of mechanical energy only occurs in shear)

$$\mu = \mu_0 \left[1 + \frac{1}{Q} \left(\frac{2}{\pi} \ln\left(\frac{\omega}{\omega_0} \right) + i \right) \right] \tag{2}$$

where μ_0 is the value of μ at some reference frequency ω_0 and the last term $i\mu_0/Q$ is the dissipation term, i being the imaginary unit [*Benjamin et al.*, 2006]. This expression reduces for frequency independent parameters to

$$\mu = \mu_0 + i\frac{\mu_0}{Q} \tag{3}$$

From this expression it is clear that the effect of Q is to change μ only slightly and the imaginary part of μ, i.e., μ_0/Q, which is a measure of the dissipation, contributes little. In order to calculate the imaginary part of μ, we define a local quality factor, q, which measures the amount of energy being dissipated within each shell and the ratio, μ_0/q, in every shell thus makes up the imaginary contribution to μ as a function of depth. In order to calculate the dissipation or equivalently the anelastic part of k_2 we employ the following scheme [J. Wahr, personal communication, 2004]. We employ the set of parameters $\{r_j, \rho_j, \mu_j, \kappa_j\}$, κ being bulk modulus, to calculate the purely elastic part of k_2 and label it k'_2. Having done this, we perturb μ in layer j from μ_j to $\mu_j + \delta\mu_j$, where $\delta\mu_j = \mu_j/q_j$ and $\delta\mu_j \ll \mu_j$. Using this new value for μ_j, μ_j, we recompute the Love number and designate it k''_2. From this we can estimate the derivative of the Love number with respect to μ in layer j as $dk/d\mu = (k''_2 - k'_2)/\delta\mu$. Then to first order in $1/Q$, the value of the Love number for an inelastic planet will be

$$\begin{aligned} k_2 &= k'_2 + i\sum_j \frac{dk_j}{d\mu_j}\delta\mu_j \\ &= k'_2 + i\delta k_2 \end{aligned} \tag{4}$$

[32] Comparing this with the expression for k_2 in the general case, i.e., $k_2 = Re(k_2) + iIm(k_2)$, we see that δk_2 makes up the imaginary contribution to the Love number. Having thus estimated the anelastic part of the Love number, the global tidal dissipation can be determined from $1/Q = Im(k_2)/Re(k_2)$.

4.4. Estimating Mass and Moment of Inertia

[33] Average density and mean moment of inertia are estimated by integration of the density profile

$$I = \frac{8\pi}{3}\int \rho(r) r^4 dr, \quad \bar{\rho} = \frac{3}{R^3}\int \rho(r) r^2 dr \tag{5}$$

where R is mean planetary radius.

5. Inverse Problem

[34] The inverse problem as posited here is strongly nonlinear and is solved using a stochastic sampling algorithm. A Markov chain Monte Carlo (MCMC) algorithm is used to sample solutions (i.e., physical configurations) of the inverse problem that both fit the observations within error and satisfy known or assumed physical a priori constraints. Briefly, the MCMC method samples the parameter space according to the posterior probability density function (*pdf*), defined as the conjunction of various *pdf*'s $\sigma(\mathbf{m}) = k\eta(\mathbf{m})\mathcal{L}(\mathbf{m})$ [*Tarantola and Valette*, 1982; *Mosegaard and Tarantola*, 1995], where k is a normalization constant, $\eta(\mathbf{m})$ describes prior information on model parameters $\mathbf{m}$ and $\mathcal{L}(\mathbf{m})$ is the likelihood function, containing information on observations and the physical laws which relate data and model parameters (for details the reader is referred to *Khan et al.* [2006a]). Let us turn to the forms of prior distribution and likelihood function.

5.1. Parameterization and the Prior Distribution

[35] The prior information is specified by a range for each model parameter as well as an assumed probability distribution for the parameter within this range.

5.1.1. Layer Thicknesses

[36] Layer thicknesses d are assumed to be uniformly distributed within certain intervals. Crustal thickness, $d_{cr} \in$ [35; 65] km, in accordance with recent estimates of the average crustal thickness of Mars [*Wieczorek and Zuber*, 2004; *Neumann et al.*, 2004], $d_M \in [d_{cr}; r_M - r_c]$, where d_M is thickness of the mantle layer, r_M is Martian radius fixed at 3389.5 km and r_c is variable core radius (see below).

5.1.2. Silicate Composition

[37] Composition c of the mantle is log-uniformly distributed within the intervals CaO $\in$ [1; 8], FeO $\in$ [5; 20], MgO $\in$ [33; 55], $Al_2O_3 \in$ [1; 8] and $SiO_2 \in$ [20; 55] (all in wt%), with the normalization constraint $\Sigma_i c_i$ = 100 wt%. These wide ranges are adopted as they are likely to encompass the concentrations of the CFMAS oxides in the Earth, Moon and silicate fraction of chondrites [*Kuskov et al.*, 2002]. As the data considered here are not very sensitive to the crust, we chose a simple parameterization using crustal density (ρ_{cr}), P and S wave velocity (V_P^{cr}, V_S^{cr}), These parameters were uniformly distributed in the intervals $\rho_{cr} \in$ [2.8; 3.2] g/cm^3, $V_P^{cr} \in$ [5.8; 6.8] km/s and $V_S^{cr} \in$ [3.2; 4.2] km/s, respectively, the latter based on PREM values and the former on estimates from recent gravity modeling [*Belleguic et al.*, 2005].

5.1.3. Temperature

[38] Temperature T is not modeled directly; rather we sample a set of geothermal gradients. For this purpose we assume the Martian geotherm to be continuous and piecewise linear, consisting of ten segments. The ten gradients are associated with ten depth segments, each of 200 km thickness in agreement with previously employed model areotherms [e.g., *Bertka and Fei*, 1997; *Longhi et al.*, 1992]. The radial thermal gradients $dT/dr = \nabla T$ in layer k are perturbed according to the scheme $\nabla T_k = \partial T_k + \epsilon\eta_k$, where ∂T_k is the thermal gradient determined in the previous iteration, ϵ is a uniformly distributed random number in the interval [−1; 1], and η_k is a constant decreasing as a function of depth to ensure that $T_{k-1} \leq T_k$.

Table 3. Summary of Model Parameters

Model Parameter	Description	No.
c	mantle composition	5
T	crust and mantle temperature	10
d_{cr}	crustal thickness	1
ρ_{cr}	crustal density	1
V_P^{cr}	crustal P wave velocity	1
V_S^{cr}	crustal S wave velocity	1
ρ_c	core density	1
r_c	core radius	1
V_S^c	core S wave velocity	1
V_P^c	core P wave velocity	1

5.1.4. Core Properties

[39] Core properties include core radius (r_c), density (ρ_c), P and S wave velocities (V_P^c, V_S^c). r_c is distributed uniformly in the interval (1000; 1900) km. The density at the top of the core (ρ_c) is assumed to be distributed uniformly in the interval, $\rho_c \in [\rho_m;\rho_{Fe}]$, where ρ_m is the value of ρ at the base of the mantle, as determined in section 4.2, and ρ_{Fe} is an upper bound on the core density and equal to 9.5 g/cm^3, in agreement with recent high pressure measurements [*Fei et al.*, 2006]. Assuming S to be the major alloying element in the core, we use the results of *Kavner et al.* [2001] (see their Figure 6), who conducted density measurements of the Fe-FeS system at high pressures (35 GPa) and temperatures (2200 K) to construct an equation of state allowing us to estimate the density as a function of pressure, temperature and S content, given a value of ρ_c. Elastic properties of the core are parameterized by single P and S wave velocities. V_S^c is assumed uniformly distributed in two intervals [0; 0.1] km/s and [3; 4] km/s, respectively, representative of the range of shear velocities in the Earth's inner and outer core. The two distributions for V_S^c, which are chosen at random (as are the S wave velocities within these), thus distinguish between solid and liquid states. P wave velocities are scaled to V_S^c using PREM values for the inner and outer core.

[40] Model parameters are summarized in Table 3 below and contained in the model parameter vector $\mathbf{m} = \{c_{ij}, T_k, d_j, \rho_{cr}, V_P^{cr}, V_S^{cr}, r_c, \rho_c, V_S^c, V_P^c\}$, which consists of 23 parameters in all. Mineralogy, density, elastic moduli, P and S-wave velocities were established at 100 km intervals in the silicate layers from the surface downward as a function of pressure, temperature and composition.

5.2. Posterior Distribution

[41] Under the assumption that data uncertainties are normally distributed and independent, the likelihood function is

$$\mathcal{L}(\mathbf{m}) \propto \prod_j \exp\left\{-\frac{\left[d_{obs}^j - d_{cal}^j(\mathbf{m})\right]^2}{2\sigma_j^2}\right\} \tag{6}$$

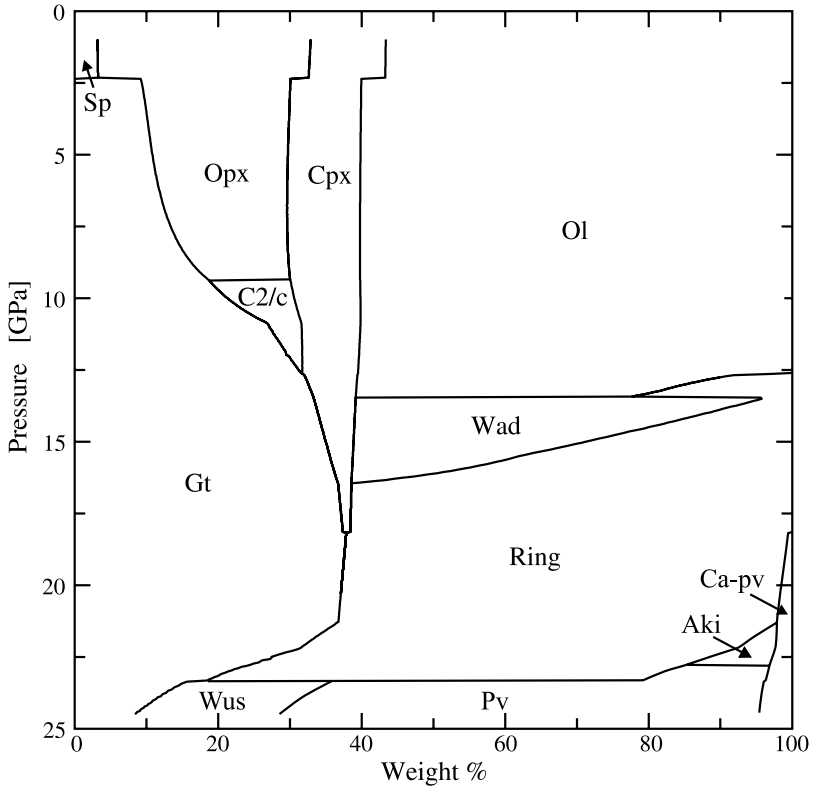

Figure 1. Computed modal mineralogy of the DW-SNC Martian composition recast in CFMAS for the areotherm of *Bertka and Fei* [1997] (Figure 5). See Table 2 for phase notation.

where d_{obs} denotes observed data, $d_{cal}(\mathbf{m})$ calculated data, $j = k_2$, Q, $\bar{\rho}$, I and σ the uncertainty on either of these.

[42] In each iteration a shell was chosen at random and subsequently all parameters pertaining to this shell were perturbed using the prior distribution as defined in the previous section. The adopted distribution has a burn-in time (number of iterations until we start retaining samples from the posterior distribution) of the order of $5 \cdot 10^3$. In all 10 million models were sampled and to ensure near-independent samples every 10^3rd model was retained for further analysis, with an overall acceptance rate of about 35%.

6. Results and Discussion

6.1. Phase Diagram

[43] The stable phases predicted for the Martian mantle are: anorthite (An), olivine (Ol), orthopyroxene (Opx), clinopyroxene (Cpx), spinel (Sp), the high-temperature monoclinic polymorph of orthopyroxene (C2/c), garnet (Gt), wadsleyite (Wad), ringwoodite (Ring), magnesiowüstite (Wus), akimotoite (Aki), perovskite (Pv), and Ca-perovskite (Ca-pv). As a test of the thermodynamic model we calculated phase proportions (Figure 1) for the composition and physical conditions investigated by *Bertka and Fei* [1997] (hereafter referred to as BF97). These proportions agree well with those determined experimentally by BF97 (their Figure 8), with the exception that here orthopyroxene and its monoclinic polymorph persist to pressures roughly 3 GPa greater than observed in the experimental system. As in the phase diagram section of BF97, we find an upper mantle consisting of ~60 (58) Ol, ~20 (19) Opx, ~10 (13) Cpx and ~10 (10) Gt to pressures of 9.5 GPa, above which Opx transforms into the high-pressure phase C2/c (all numbers are in wt% and parentheses refer to values by BF97). Up until about 12 GPa Ol, CPx, C2/c, Gt (majorite) coexist in modal abundances of 60 (58), 10 (32, Cpx by BF97 here refers to our Cpx + C2/c), 5, 25 (10, by BF97 majorite only occurs below the transition zone), with C2/c disappearing and Ring appearing at ~12.5 GPa (γ-Sp). The latter occurs at a slightly lower pressure than determined by BF97 (13 GPa). The region around 14 GPa marks the onset of the Martian mantle transition zone, corresponding to the 410 km transition zone discontinuity in the Earth due to the transformation Ol $\rightarrow$ β-Sp. In concurrence with BF97, at ~14 GPa Ol is replaced by Wad (β-Sp) at 60 (53) wt%, which persists up to around 17 GPa, at which pressure Cpx/C2/c and Wad are replaced by Ca-pv and Ring, respectively. The phases coexisting up to around 21.5 GPa are Ring and majorite, at 60 (55) and 38 (45) wt%, respectively, with small amounts Ca-pv (~2 wt%). Between 21.5 and 23 GPa Aki is stable, a phase not observed by BF97. At pressures above 23 GPa, BF97 in agreement with our results find a lower mantle principally made up of majorite Gt, Wus, and Pv, as all Ring transforms. The phases occur at levels of 10 (10), 20 (15), and 68 (75), respectively. Small amounts of Ca-pv (<5 wt%) are also present. The densities predicted for the BF97 model are systematically higher than reported by *Bertka and Fei* [1998a] (Figure 2), but the density changes found by *Bertka*

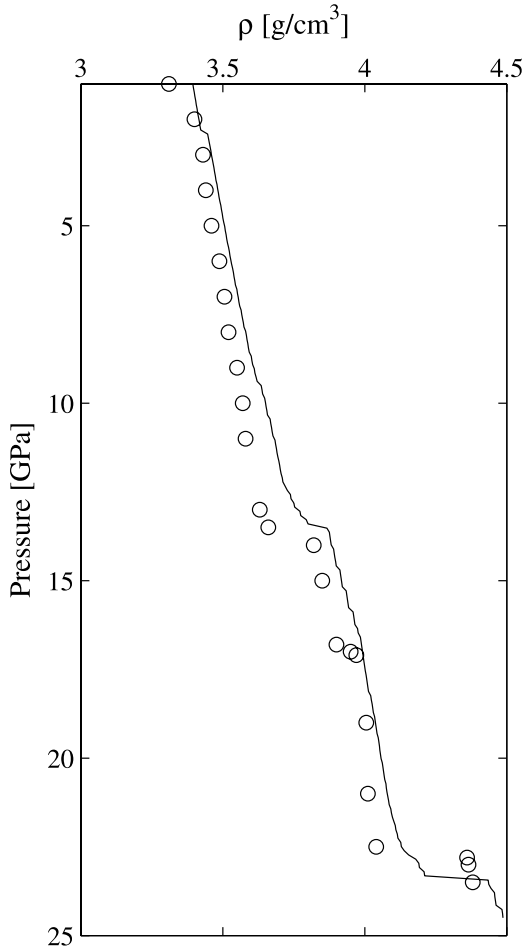

Figure 2. Computed density profile of the Martian mantle with the DW-SNC model composition. Circles are the mantle densities calculated by *Bertka and Fei* [1998a] from their experimental determinations. Crustal part is not shown.

and Fei [1998a] at ~13 and ~23 GPa, marking the midmantle and lower mantle transition, respectively, are reproduced.

[44] Differences between our modal abundances and density profile, and those of Bertka and Fei are related mostly to differences in composition. In particular, we attribute the discrepancy between our density profile and that of Bertka and Fei to the omission of Na_2O, the lightest oxide component, from our CFMAS version of Bertka and Fei's model composition. The composition employed by BF97 contains 0.5 wt% Na_2O, which, when reinterpreted in terms of CFMAS, results in a slightly different composition (2.55, 19.15, 32.24, 2.36, 43.71; all numbers in wt%).

[45] Although the lower mantle predicted for the BF97 model is dominated by perovskite-structure silicates, the stability of these silicates depends strongly on temperature and pressure conditions at the CMB, pressure being determined by core size and composition. Large cores will result in a lower mantle that is either thin or absent altogether; whereas higher temperatures will tend to stabilize Pv at lower pressures. The existence of a perovskite-dominated lower mantle is thus sensitive to the physical conditions at the CMB.

6.2. Predicted Data

[46] Sampled marginal posterior data distributions are displayed in Figure 3, demonstrating our ability to fit data within uncertainties.

6.3. Composition, Thermal State, and Mantle Mineralogy

[47] Sampled prior and posterior bulk silicate mantle compositions are shown in Figures 4a–4g, while Figure 4h displays bulk sampled Fe/Si ratios. For comparison, we have also included the DW-SNC composition and estimates of Fe/Si ratios for chondritic meteorite groups. For all CFMAS elements significant differences are palpable among sampled prior and posterior *pdf*'s, implying that inversion of the data set considered here can indeed be used to constrain the mantle composition. A Martian mantle with a low refractory element budget as suggested by the SNC's also seems to be the case here, where most probable CaO and Al_2O_3 contents and element ratios are found to be around 2.2 wt%, 2.5 wt% and 1, respectively. FeO enrichment, as implied by DW-SNC, is also prevalent here, with most of the probability contained in the range between 15 and 20 wt%, and most probable FeO contents of ~17wt%. The amount of MgO is somewhat higher in comparison to DW-SNC, with most probable values around 32–35 wt%, while most probable SiO_2 values are around 44 wt%, in close agreement with DW-SNC. Sampled bulk silicate molar Mg# and Mg/Si ratios (Figures 4f and 4g) are seen to agree well with the estimate of DW-SNC, while sampled bulk Fe/Si ratios (Figure 4h) are inconsistent with the assumption of DW that the composition of Mars can be constrained to that of CI chondrites. The agreement between our derived silicate compositions and the DW-SNC model is remarkable, given that our compositions were obtained without referring to the SNC's. The results are summarized in Table 4 with some additional literature estimates and average meteorite compositions of *Jarosewich* [1990].

[48] Sampled prior and posterior areotherms are displayed in Figures 5a and 5b. In Figure 5b we have also included the temperature data points used by BF97 in their experimental runs. At first glance there is little difference between prior and posterior *pdf*'s. However, a closer look reveals small, but subtle differences. Down to depths just above the transition zone, the posterior *pdf*'s are narrower and from the transition zone down to the CMB, the *pdf*'s have been displaced in comparison to the prior *pdf*'s. Most probable CMB temperatures are around 1800°C, which is somewhat higher than suggested by recent thermal history models [e.g., *Williams and Nimmo*, 2004; *Hauck and Phillips*, 2002].

[49] Our predicted mantle mineralogy (Figure 6) is similar to the one already discussed in section 6.1, and generally agrees with earlier results. The upper mantle is largely composed of Ol, Opx, Cpx and an aluminous phase, An, Sp or Gt. At a depth of approximately 800 km, Opx transforms into the high pressure phase C2/c, which is present in somewhat greater amounts than predicted by BF97. The transition zone occurs at about 1100 km depth and coincides with the Ol → Wads + Ring transition. Below the transition zone the mantle is principally made up of majorite Gt, Wads, Ring and from 1400 km depth also Aki. This mineralogy is consistent with that predicted by Martian

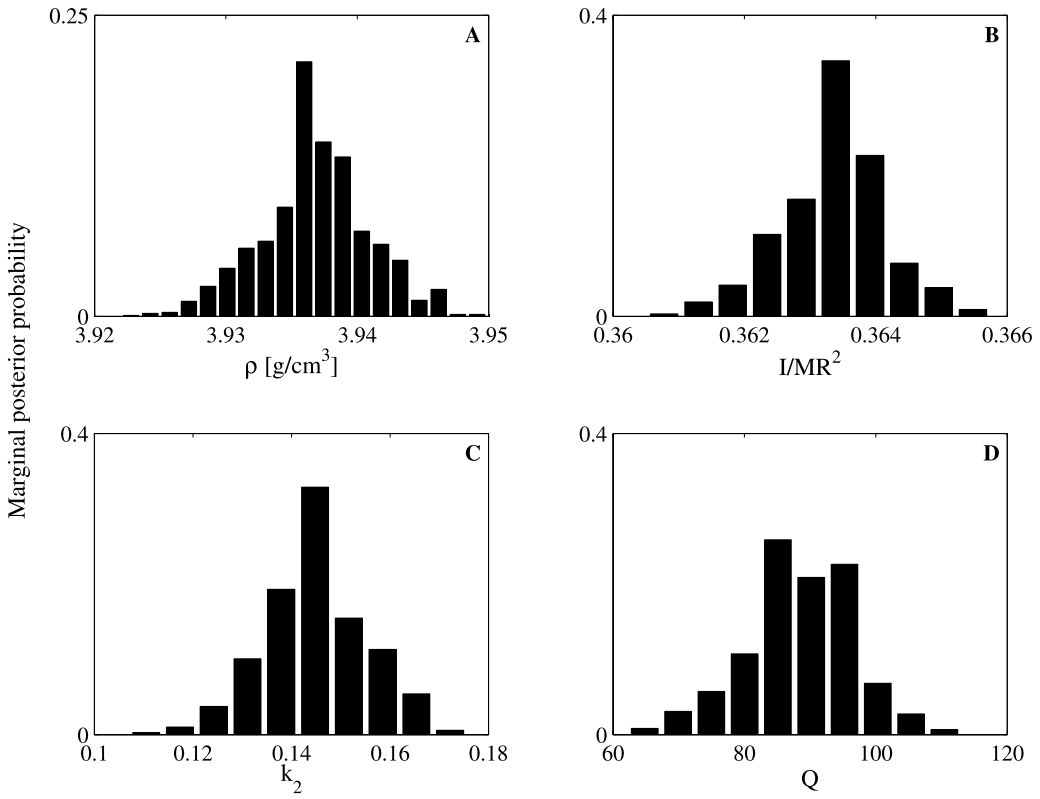

Figure 3. Marginal posterior data fit to mean density (a), mean MOI (b), second degree tidal Love number (c), and tidal dissipation (d). The observed data are given in Table 1.

magma ocean evolution models [*Elkins-Tanton et al.*, 2003, 2005].

[50] As already pointed out, the transition to a lower mantle composed of silicate perovskite is strongly dependent upon both pressure and temperature conditions at the CMB. Here we find most probable CMB pressures around 20–21 GPa, implying that a lower mantle transition to perovskite structure silicates does not occur in the vast majority of models. This can be quantified, as a probabilistic measure of occurrence of a given feature in the posterior models can be obtained from [e.g., *Mosegaard*, 1998]

$$\mathcal{R}(\Omega, f) \approx \frac{1}{N} \sum_{\{n|\mathbf{m}_n \in \Omega\}} f(\mathbf{m}_n) \tag{7}$$

where $f(\mathbf{m})$ is a given function of the model parameters $\mathbf{m}$, Ω is an event or subset of the model space containing the models of current interest, i.e., those models where Pv occurs, and N is the total number of samples taken from Ω. Application of equation (7) results in <2% of all sampled models with mantle pressures high enough for Pv to appear and thus for a lower mantle transition to occur. This result weakens the hypothesis that perovskite structure silicates are present as a layer above the CMB as assumed in most previous studies [e.g., *Longhi et al.*, 1992; *Bertka and Fei*, 1997, 1998a; *Elkins-Tanton et al.*, 2003, 2005]. The absence of a perovskite layer above the CMB can potentially be important for mantle convection, as the endothermic phase transformation associated with this layer has figured as a means of organizing convection into superplumes to explain Tharsis and Elysium [e.g., *Harder*, 2000; *Van Thienen et al.*, 2006].

[51] The presence of a lower mantle in earlier studies hinged on a number of modeling assumptions, which could not be independently determined, including crustal density and thickness, and in particular core composition and size, and not least the thermal profile adopted. As discussed by *Bertka and Fei* [1998a] varying the crustal thickness in the range from 42 to 140 km, with a fixed density of 2.7 g/cm^3 assuming a DW-SNC mantle composition and a core composed of Fe-14 wt% S (radius ~1450 km), changed the thickness of the perovskite-bearing layer from 100 to 0 km.

6.4. Physical Properties: Density, *P* and *S* Wave Velocity

[52] The variations of density, P and S wave velocity with depth are shown in Figures 7a–7c. The figure also shows the experimentally determined density model of *Bertka and Fei* [1998a], model M13 obtained by *Zharkov and Gudkova* [2005], Kuskov and Panferov's Martian upper mantle model, as well as the V_P and V_S model calculated using the DW-SNC model composition and the areotherm of *Bertka and Fei* [1997] (see section on Phase Diagram for details).

[53] Shear wave velocities, in particular, are seen to remain more or less constant as we are moving down through the thermal boundary layer and into the upper mantle, whereas density and P wave velocity increase continuously. This shows that S wave velocities are relatively more affected by temperature in the upper mantle than are P wave velocities, in agreement with what is observed in the Earth's upper mantle [e.g., *Stixrude and Lithgow-Bertelloni*, 2005]. S wave velocities do not increase significantly until a

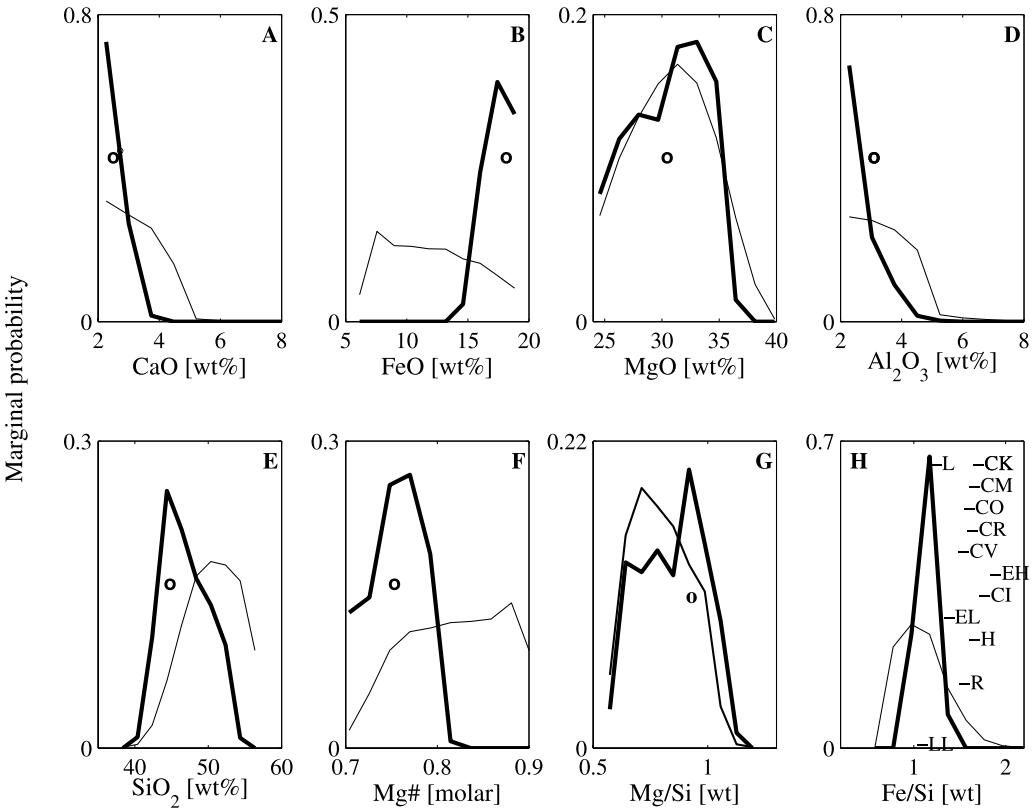

Figure 4. Prior (thin line) and posterior (thick line) marginal *pdf*'s depicting sampled bulk silicate compositions for the CFMAS elements (a-e), bulk silicate Mg# (f), bulk silicate Mg/Si ratio (g), and bulk Fe/Si ratio (h) as well as Fe/Si ratios for chondritic meteorite groups (from the compilation of *Burbine and O'Brien* [2004]). In Figures 4a–4g circles indicate the SNC model Martian composition of DW. Note that as the elemental concentrations are plotted in wt% and not as log(wt %), their distributions will appear skewed.

depth of ~800 km is reached, at which point *S* wave velocities increase by around 3–5%. This transition, also observable in the density profiles, marks the disappearance of Opx and the appearance of C2/c and significant amounts of Gt, both of which as individual phases have higher velocities and densities. The V_S profile calculated on the basis of the CFMAS-recast DW-SNC composition and BF97 areotherm also shows this transition. This is the only region in which our estimated densities are higher than those obtained by *Bertka and Fei* [1998a]. Down to the midmantle transition zone at ~1100 km depth, all physical properties are seen to rise further, including *S* wave velocities, reflecting the importance of pressure effects on wave velocities, in contrast with the upper mantle where temperature effects are relatively more important. A major discontinuity at the midmantle transition is seen in all three physical properties as upper mantle minerals transform into majorite Gt, Wad and Ring. For *P* and *S* waves, velocity increases of around 6–9% are found, while density is found to increase by around 5%, which is similar to what is obtained in the Earth's transition zone (410 km depth) [e.g., *Stixrude and Lithgow-Bertelloni*, 2005]. The midman-

Table 4. Summary of Derived Bulk Compositions (Most Probable Values), Various Literature Estimates and Some Average Meteorite Compositions From *Jarosewich* [1990][a]

Study	CaO	FeO	MgO	Al_2O_3	SiO_2	Mg#
This study	2.2	17	33	2.5	44	0.77
Morgan and Anders	5.2	15.8	29.8	6.4	41.6	0.77
Wänke and Dreibus (SNC)	2.4	17.9	30.2	3	44.4	0.75
Sanloup et al. (EH45:H55)	2	17.7	27.3	2.5	47.5	0.72
Sanloup et al. (EH70:H30)	2	11.4	27.3	2.5	51	0.8
Lodders and Fegley	2.35	17.2	29.7	2.9	45.4	0.75
CM2	1.9	22.1	19.9	2.2	28.9	0.62
CV3	2.6	26.8	24.6	3.2	34.0	0.62
H	1.7	10.3	23.3	2.1	36.6	0.8
L	1.9	14.5	24.7	2.3	39.7	0.75
LL	1.9	17.4	25.2	2.2	40.6	0.72

[a]All values are in wt%.

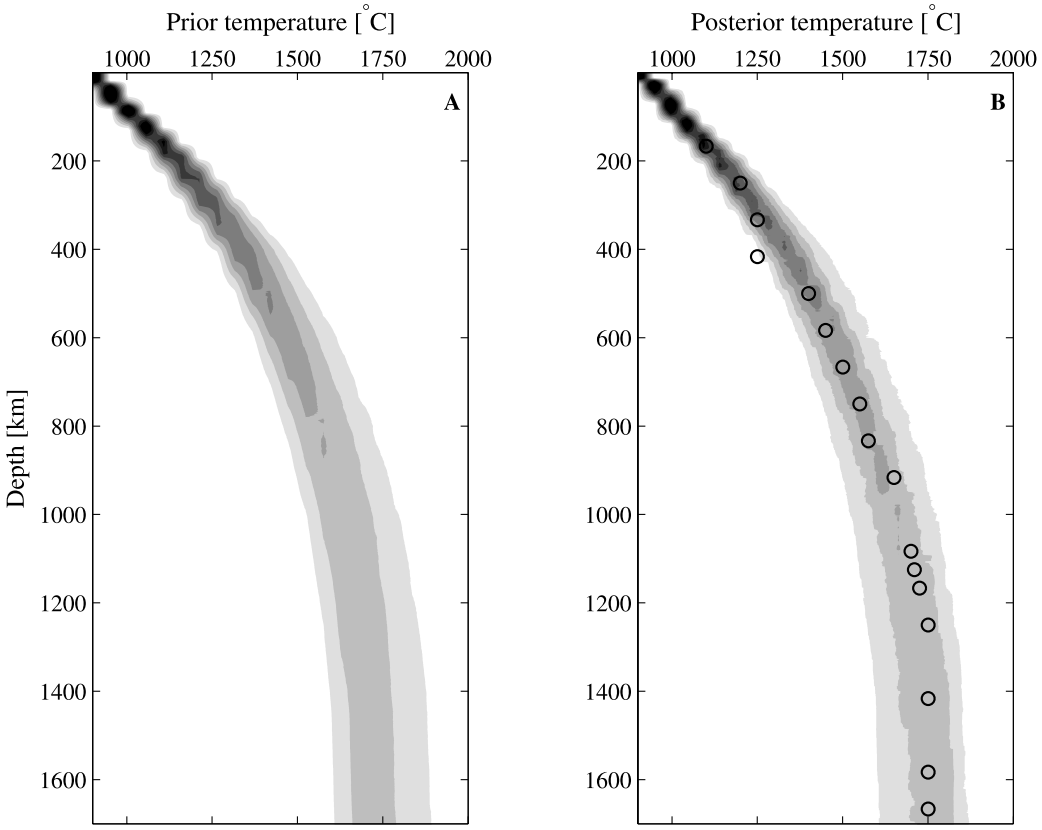

Figure 5. (a) Prior and (b) posterior sampled mantle areotherms. At the 30 fixed depth nodes a histogram reflecting the marginal probability distribution of sampled temperatures is calculated. By lining up these marginals, temperature as a function of depth can be envisioned as contours directly relating their probability of occurrence. Shades of gray between white and black indicating, respectively, least and most probable outcomes, with each contour line defining an equal-sized probability density interval for the distributions. The thermal model conditions from *Bertka and Fei* [1997] are indicated by circles.

tle transition is extant in all the other models shown in Figure 7 and is seen to occur at depths which are within the uncertainties of our models. Throughout the midmantle and down to the CMB, physical properties continue to increase as pressure rises with depth. Further significant increases in physical properties related to a lower mantle transition, as Ring and Gt transform to Wus and Pv, occur in the *Bertka and Fei* [1998a] model at an approximate depth of 1950 km (corresponding to 23.5 GPa), but not in ours, nor in that of *Zharkov and Gudkova* [1997]. The absence of a lower mantle transition in our models is directly related to the large core radii sampled (see core section below).

[54] The variations in physical properties obtained here are caused principally by changes in major element composition and temperature, while effects arising from the presence of melt, attenuation and compositional heterogeneity are potentially important but beyond the scope of the present study. Also, effects arising from minor elements (e.g., Na_2O, TiO_2 and Cr_2O_3) are unlikely to lead to significant changes in velocities, but will mostly affect depths of phase transformations [*Stixrude and Lithgow-Bertelloni*, 2005].

6.5. Core Size, Composition, and State

[55] One of the presently least constrained parameters is the size of the Martian core. It is, however, very important to assess this parameter, since it provides crucial constraints on mantle and core composition in addition to determining whether a lower mantle exists or not. Assuming a core composition of Fe-14 wt% S, [*Fei and Bertka*, 2005] found CMB pressures of ~23 GPa, which, depending on the nature and physical state of the mantle, corresponds to ~1800 km depth [*Bertka and Fei*, 1997]. *Yoder et al.* [2003] observationally constrained core radius to be between 1520 km and 1840 km for a core composed of Fe-FeS, while *Zharkov and Gudkova* [2005] estimated core radii in the range 1620–1800 km for an Fe-S-H core. Our previous discussion has already shown that the CMB is more likely to occur at pressures of ~21 GPa, corresponding to larger core sizes than envisaged by *Fei and Bertka* [2005] for example. In Figures 8a and 8b are shown prior and posterior sampled core densities as a function of core radii. The relatively flat prior *pdf* has been strongly narrowed as data are taking into account, and point to a most probable core radius and density of ~1680 km and ~6.7 g/cm^3, respectively. In Figure 8b are also indicated experimentally determined densities for various Fe-S configurations adopted from *Kavner et al.* [2001]. Assuming S to be the only major alloying element, the plot suggests a Fe-S core composition containing ~22–25 wt% S. Effects of Ni as a core constituent are not considered in the present discussion as *Hixson et al.* [1990] have shown that Ni has little influence on the density of liquid iron and its

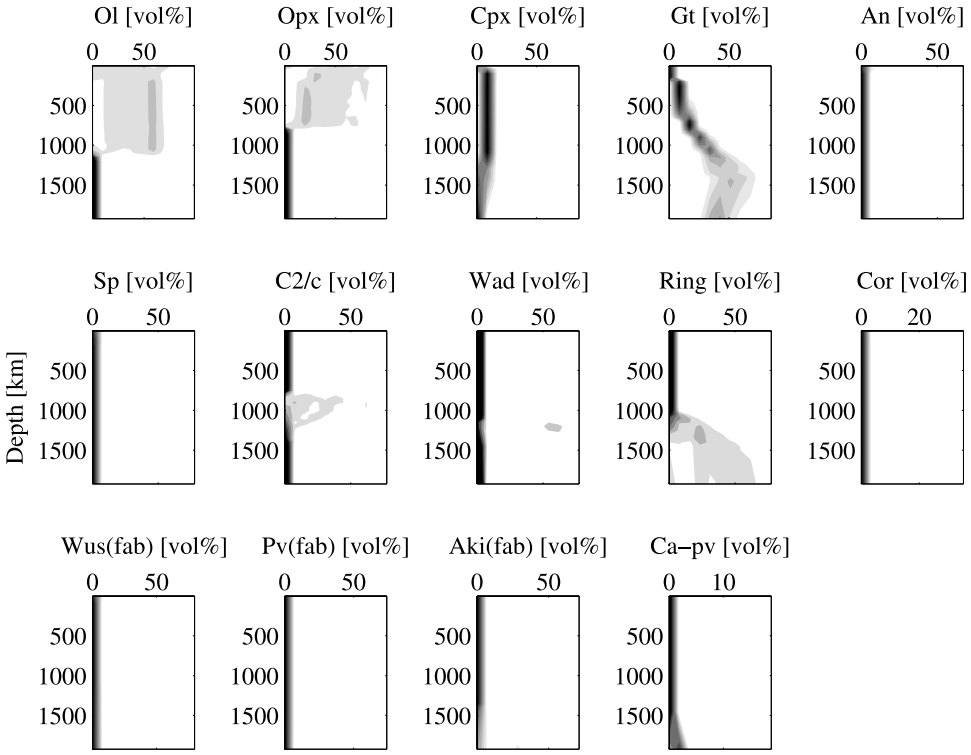

Figure 6. Posterior marginal modal mineralogy as a function of depth down to the CMB. In some of the plots, e.g., Wus and Pv, minerals do not seem to be stable. This is because these minerals are only stable for a few models. See main text for further discussion. Shades of gray as in Figure 5.

temperature dependence. That adding Ni to the Fe-S system has little effect has also been recorded in experimental investigations of the Fe-S and (Fe,Ni)-S systems conducted recently by *Stewart et al.* [2007]. We have compiled some previous estimates of core size in Table 5 below, including their fit to data. Most of the tabulated models assume (1) a crustal thickness and density of 50 km and 3 g/cm^3, respectively, in general agreement with the average values obtained

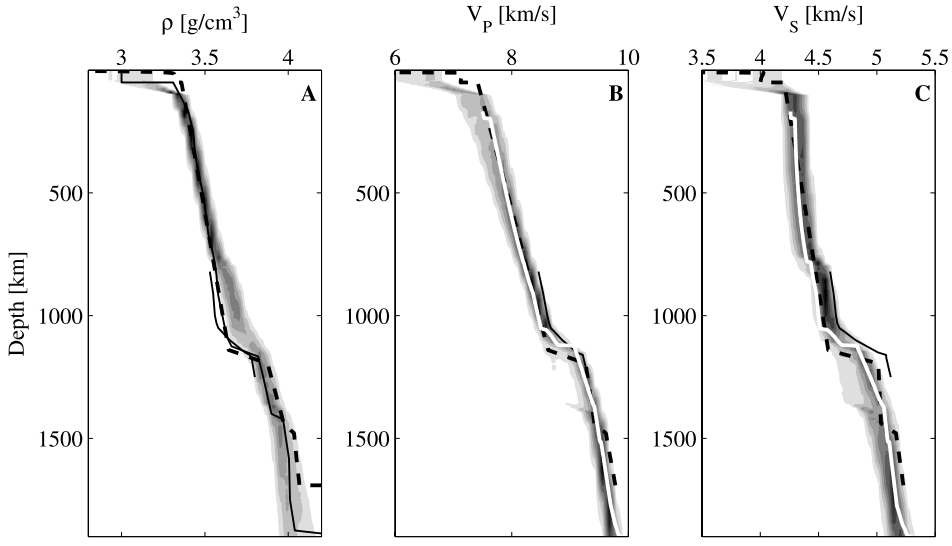

Figure 7. (a) Posterior marginal mantle physical properties in the form of density (a), (b) *P wave* velocities, and (c) *S*-wave velocities as a function of depth. The solid line in Figure 7a depicts the density model of *Bertka and Fei* [1998a] also shown in Figure 2, dashed lines in Figures 7a–7c is model M13 of *Zharkov and Gudkova* [2005], short solid lines in Figures 7a–7c is the model of *Kuskov and Panferov* [1993] and white lines in Figures 7b–7c are V_P and V_S calculated on the basis of the CFMAS-recast DW-SNC model composition (see text and caption of Figure 2) and the areotherm of *Bertka and Fei* [1997] (see Figure 5). Shades of gray as before.

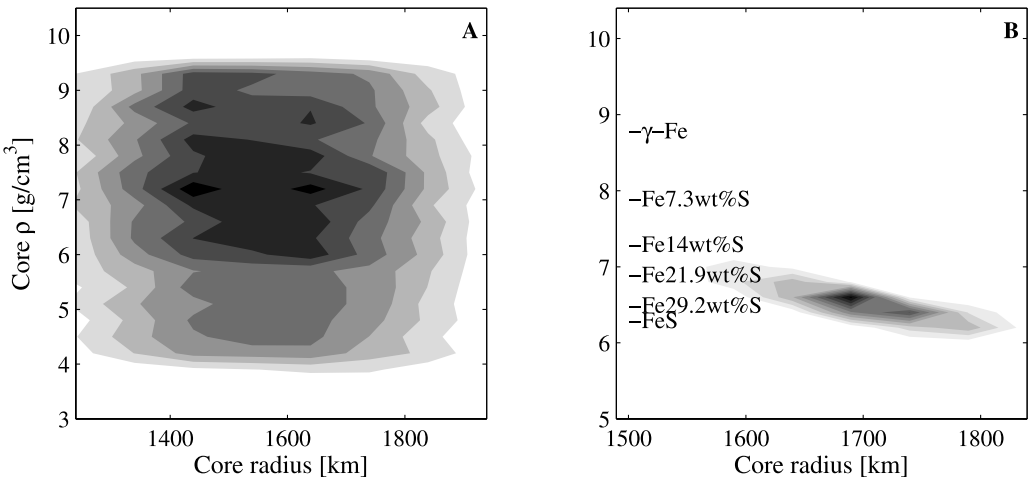

Figure 8. (a) Prior and (b) posterior two-dimensional marginal posterior *pdf*'s showing the correlation between core radius and core density. In Figure 8b are added experimental density determinations for the Fe-FeS system from *Kavner et al.* [2001]. Shades of gray as before.

here, and (2) a core composition with ~14 wt% S. This table shows that while some estimates are within ours, they result in a data fit that, in most cases, barely fit present-day observations.

[56] As noted previously, there is considerable evidence that the Martian core was fluid some 4 Ga ago. Convective motions driven by a super-adiabatic heat flow out of a liquid metal core [*Stevenson*, 2001] would generate a once global Martian magnetic field, which is held to be the source of the highly magnetised rocks in the southern Martian hemisphere observed by MGS [*Connerney et al.*, 1999; *Acuña et al.*, 1999]. The crust is envisioned to have become magnetised as it crystallised in the presence of the magnetic field generated short-lived dynamo (~0.5 Ga). Subsequent secular cooling and crystallisation of the liquid core, in analogy with the Earth's core, and/or a possible change in mantle convection style [e.g. *Stevenson*, 2001], is thought to result in cessation of dynamo action close to 4 Ga ago. This is in line with the present-day observation of a no longer existing global magnetic field as well as the observation by *Weiss et al.* [2002] that carbonates in ALH84001 acquired their magnetisation prior to 3.9 Ga. With regard to the onset of the Martian dynamo, *Schubert et al.* [2000] have proposed an alternative scenario to an early and short-lived one. They argue that dynamo action postdates emplacement of bulk of the southern hemispheric crust, based on the absence of magnetic anomalies at the Hellas and Argyre impact basins. Such magnetic anomalies would have been expected to be present if the crust had been magnetised prior to the impacts. Instead they suggest that the southern magnetised regions are due either to later magmatic additions to the crust (when dynamo action had commenced), or thermal reworking of older, possibly more localised, crust. Either way, core crystallisation is believed to be a main source in powering the Martian dynamo. However, recent experimental investigation of *Stewart et al.* [2007] suggests that the Martian core is likely to be entirely liquid at present, and that the mechanisms of convection as well as solidification are unlike what is expected based on terrestrial experience.

[57] Our results also suggest, both directly and indirectly, a present-day liquid Martian core (at least of its outer part).

Table 5. Summary of Some Recent Core Size and Compositional Estimates, and Their Geophysical Predictions[a]

Model	Core Size, km	Core ρ, g/cm^3	Core Composition	Estimated Data
This study	1680	6.7	75–78 wt% FeNi, 22–25 wt% S	see Table 1
Zharkov and Gudkova (M13)[b]	1699	6.5	14 wt% S, 50 mol% H	$I = 0.3649$ $k_2 \sim 0.141$
Zharkov and Gudkova (M9)[b]	1568	7	80 wt% FeNi, 20 wt% S	$I = 0.3654$ $k_2 \sim 0.122$
Zharkov and Gudkova (M10)[b]	1816	5.9	64 wt% FeNi, 36 wt% S	$I = 0.3674$ $k_2 \sim 0.161$
Sohl et al.[c]	~1630	7.5	n.d.	$I = 0.3635 \pm 0.0012$ $k_2 = 0.0122$
Yoder et al.[d]	1520–1840		25% < Fe/(Fe-FeS) < 75%	$k_2 = 0.145 \pm 0.017$ $C = 0.365 \pm 0.0012$
Kavner et al.[d]	1480	7.3	85.8 wt% FeNi, 14.2 wt% S	$C = 0.366$
Sanloup et al. (model I)[e]	1710 ± 5	6.9	83.8 wt% FeNi, 16.2 wt% S	$I = 0.361 \pm 0.002$
Sanloup et al. (model II)[e]	1865 ± 5	6.87	82.6 wt% FeNi, 17.4 wt% S	$I = 0.352 \pm 0.002$
Bertka and Fei[f]	1421	6.8	85.8 wt% FeNi, 14.2 wt% S	$I = 0.366$
Lodders and Fegley	1630	7.27	89.4 wt% FeCoNi, 10.6 wt% S	$C = 0.367$
Longhi et al.[g]	1695 ± 70	6.8	85.8 wt% FeNi, 14.2 wt% S	$C = 0.353$

[a]Results quoted from the present study refer to most probable values.
[b]$\rho_{cr} = 3.2$ g/cm^3, $d_{cr} = 50$ km.
[c]$\rho_{cr} = 3.1$ g/cm^3, $d_{cr} = 50$ km.
[d]$d_{cr} = 50$ km.
[e]$\rho_{cr} = 3$ g/cm^3, $d_{cr} = 40$ km.
[f]$\rho_{cr} = 3$ g/cm^3, $d_{cr} = 50$ km.
[g]$\rho_{cr} = 2.7$ g/cm^3, $d_{cr} = 100$ km.

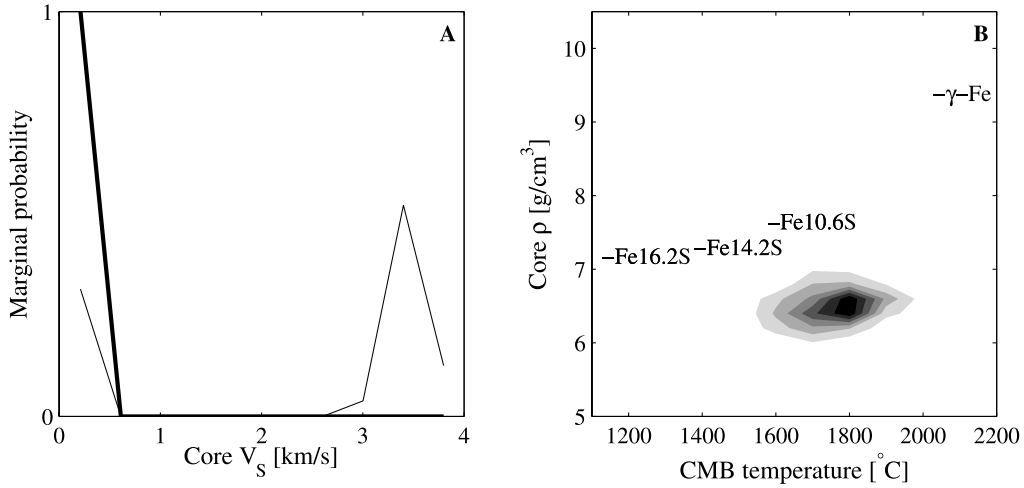

Figure 9. Additional core properties (a) depicts sampled prior (thin line) and posterior (thick line) marginal *pdf*'s for sampled *S* wave velocities in the core. Note that the posterior *pdf* is flat for velocities expected of solid core material. Figure 9b shows sampled posterior core densities as a function of CMB temperatures with experimental determinations of melting temperatures for a number of compositions in the Fe-S system included (from *Stewart et al.* [2007]). Shades of gray as before.

The results are summarized in Figure 9. Figure 9a displays prior and posterior *pdf*'s for sampled core *S* wave velocities. The posterior *pdf* is seen to be flat above 0.1 km/s in comparison to the prior and indicates that in order to fit data only low *S* wave velocities (<0.1 km/s) are sampled. Such low *S* wave velocities are interpreted as implying a fluid core. In addition, Figure 9b shows sampled posterior CMB temperatures as a function of core densities. On this figure are added melting temperatures of various compositions in the Fe-S system as determined experimentally by *Stewart et al.* [2007]. Our most probable CMB temperatures are found to be ~1800°C (for our most probable Fe-S compositions containing >20 wt% S) and are much higher than the melting temperatures determined for the composition with the highest S content (Fe-16.2 wt% S). This, in addition to, and independent of Figure 9a, suggests a presently liquid Martian core.

[58] *Stewart et al.* [2007] employed the experimentally determined eutectic melting temperatures and compositions of the Fe-S system at pressures equivalent of the center of Mars to constrain the mechanism by which a Martian core would crystallize, as the planet steadily cools. They determined eutectic melting temperatures and compositions of the Fe-S system at the CMB (23 GPa) to be ~1300 K and 16 wt% S, respectively, while at the center of Mars (40 GPa), these changed to ~1500 K and 12 wt% S, respectively. Depending on whether the actual core composition is on the Fe-rich or S-rich side relative to the eutectic, determines the mechanism by which the core solidifies. In case of an Fe-rich composition crystallization would commence at the CMB, leading to a snowing-core hypothesis, where it is envisaged that solid Fe-Ni droplets precipitate through the S-bearing liquid forming an inner Fe-Ni core and an outer core that becomes progressively enriched in S. Is the composition S-rich relative to the eutectic, the core would grow from the centre, and unlike in the Earth first crystallize an inner core of $(Fe,Ni)_3S$ and an outer core that would evolve toward a final composition composed of (Fe, Ni) and Fe_3S. If indeed the Martian core contains >20 wt% S, as suggested by our results, this implies the crystallization of a sulphide inner core. In order to explain the existence of a magnetic field that magnetized the highland rocks some 4 Ga ago in the absence of an inner core as in Earth, entails a strongly convecting fluid core, which subsequently, and possibly because of a change in convection pattern, shut down.

6.6. Implications for Bulk Composition

[59] There is considerable evidence for elemental and isotopic differences among the terrestrial planets [e.g., *Taylor*, 1999], suggesting the presence of local feeding zones from which they formed, and therefore possibly different building blocks. In the two-component accretion model of DW, Mars is assumed to have accreted homogeneously from a reduced and oxidized component, that are believed to originate within the proximity of the Earth and asteroid belt (CI chondrites), respectively. Mars accreted roughly equal proportions of the two components (the oxidized component contains all elements including volatiles in CI abundances), and at the same time, because of its location at the boundary between the two regions. In contrast, the Earth accreted heterogeneously, first accumulating material from its neighborhood and only subsequently sweeping up material from the asteroid belt, which had been transferred to the inner regions as Jupiter over time increased velocities and eccentricities of asteroidal material. Terrestrial planet formation models showed that the inner solar system planets were likely to have accreted material from all portions of the disk between 0.5 and 2.5 AU and beyond rather than from local feeding zones [*Wetherill*, 1994]. More recently, *Chambers* [2001] found that while considerable amount of radial mixing of material occurred, a compositional gradient nonetheless ensued out to 2 AU, resulting in planets retaining some form of memory of the initial distribution of parent material, in accordance with earlier suggestions by *Wetherill* [1994]. In particular, the models showed that Mars was made up mostly of material emanating from the outer zone, meaning that Mars could

have accreted large parts of asteroidal material, unlike Earth and Venus which were found to have accumulated material from several zones. So what are the possible building blocks of Mars made of?

[60] The CI Fe/Si ratio is 1.71 [*Wasson and Kallemeyn*, 1988] and the DW-SNC model composition assumes a Martian CI Fe/Si ratio. This, however, is not implied by our results here, as we find most probable bulk Fe/Si ratios around 1.2 (Figure 4h), nor by earlier analyses. *Bertka and Fei* [1998b] (hereafter BF98), for example, computed Fe/Si ratios for a number of different Martian core compositions (Fe, FeS, Fe-S, FeH, Fe_7C_3), using a mantle density profile based on DW-SNC, and found the Fe/Si ratio to vary from 1.3 to 1.5 (crustal density was fixed at 3 g/cm^3, while crustal thickness and core size were varied so that the models fit the polar MOI value of 0.3662). These values for the bulk Fe content, i.e., that contained in core, mantle and crust, to bulk silicate Si content, is lower than 1.71. BF98 noted that the difference between their Fe/Si estimates and that of DW was because the mass fraction of an Fe core with 14 wt% S only made up 13.7–19 wt%, in comparison to 21.7 wt% for the DW-SNC model. For a Fe-14 wt% S core, we find core mass fractions between 15–17.5 wt%, in agreement with BF98. The low Fe/Si ratios obtained here, which are found without any reference to the composition of the SNC's and thus independently of BF98, accentuates the conclusion, that the CI chondrite accretion model for deriving Mars is incompatible with a SNC-like mantle composition and the available geophysical data. Having discarded the CI chondrites as possible building blocks, how about the other known chondrites?

[61] Figure 4h indicates that the ordinary chondrites, in particular L and LL, are possible candidates. Indeed, a perusal of the compilation of the chemical composition of meteorites by *Jarosewich* [1990] (average compositions for a number of chondrites are given in Table 4) reveals that most major element compositions of L and LL chondrites are well within our *pdf*'s (Figures 4a–4e). Similar conclusions were also drawn in the modeling approaches by *Kuskov and Kronrod* [2001] and *Burbine and O'Brien* [2004], while somewhat different conclusions were reached in the experimental work of *Agee and Draper* [2004]. They investigated the major element compositions of partial melts of a chondritic (Homestead L5) model Martian mantle, i.e., compositionally akin to DW-SNC, at high pressure and temperature, to determine if the major element abundances of Martian basalts or their parent magmas could be derived from a model Martian mantle composition at high pressure. While their experiments showed that DW-SNC and Homestead were able to produce the CaO/Al_2O_3, CaO and Al_2O_3 values of Martian parent magmas by high-pressure partial melting and a second stage of olivine fractionation, they found that the partial melts of Homestead were too FeO-rich to match the values observed in SNCs and their calculated parent magmas. On the basis of these results Agee and Draper suggest that Martian parent magmas could possibly be derived from a bulk mantle composition such as the H chondrites, which have lower FeO contents and higher Mg#s than DW-SNC and Homestead.

[62] For completeness, we would like to observe that *Zharkov and Gudkova* [2005] find either bulk nonchondritic or chondritic (CI) Fe/Si ratios, depending on whether the core is composed of Fe-S or contains H in addition to S. For a core containing only S, bulk Fe/Si ratios between 1.3 (Fe-0 wt% S) and 1.4 (Fe-20 wt% S) are obtained, in overall agreement with our and previous results. However, is H added to the core composition, a scenario favored by Zharkov and Gudkova based on the planetary accretion model of *Zharkov* [1996] mentioned earlier, core radius is found to increase and so is core mass fraction as well as bulk Fe/Si ratio for a given value of the S content and mantle Mg#. Bulk Fe/Si ratios vary from 1.35 (0 mol% H) to 1.79 (70 mol% H, both 14 wt% S and Mg# 0.75), corresponding to core mass fractions of 19.3–23.4 wt%. On the basis of these results the authors conclude that consideration of the data by Yoder et al. leads to a preferred Martian model which is closer to having a bulk CI Fe/Si ratio. While Zharkov and Gudkova rightfully note in their discussion that the conclusions drawn by BF98 were premature given the few constraints BF98 were able to impose on core size, our conclusion reached independently of BF98, nonetheless support the contention of a bulk nonchondritic Fe/Si ratio. While we have not considered effects of adding H to our core composition, we would like to note that although the study by *Zharkov and Gudkova* [2005] is thorough with attention to detail, it is not an inversion and the models shown are but a few of possibly many models with different combinations of parameters that will fit data. For example, quantifying effects of varying the unknown areotherm, which will obviously change mantle physical structure and core properties, are not considered.

6.7. Model Resolution and Data Sensitivity

[63] From the foregoing discussion it has been indicated that in previous studies [e.g., *Sohl and Spohn*, 1997; *Bertka and Fei*, 1998a; *Yoder et al.*, 2003; *Sohl et al.*, 2005] trade-offs between certain parameters, which could not be determined independently and thus had to be assumed, exist. For example, *Bertka and Fei* [1998a] discussed how values adopted for crustal thickness and density were influential in determining whether a lower mantle was present or not. This is further exemplified in the study by *Sohl et al.* [2005]. Their Figures 3 to 6 reveal a significant trade-off between crustal thickness and parameters pertinent to the mantle (density, Mg#, Mg/Si), bulk planet (Fe/Si) as well as data (k_2 and I). Within the present thermodynamic context we are not faced with this crustal trade-off problem, nor that associated with choosing a different areotherm, as the derived crust and mantle physical structure, and whence core, are direct consequences of the proposed areotherm and composition. Our top-down thermodynamic approach ensures that what is on top determines what is below.

[64] Aspects that are important to address when making inferences from inverse calculations include data sensitivity and model parameter resolution. The issue of model parameter resolution has essentially already been addressed through the notable differences between prior and posterior *pdf*'s displayed hitherto. However, in order to investigate in detail the amount of information contained in the individual data sets, we conducted separate inversions and summarized the information in Figure 10. The plot shows 2D marginal prior and posterior *pdf*'s correlating core density and radius for inversions of only k_2 and Q (Figure 10a), and only $\bar{\rho}$ and I (Figure 10b). We can see that as we add more information in

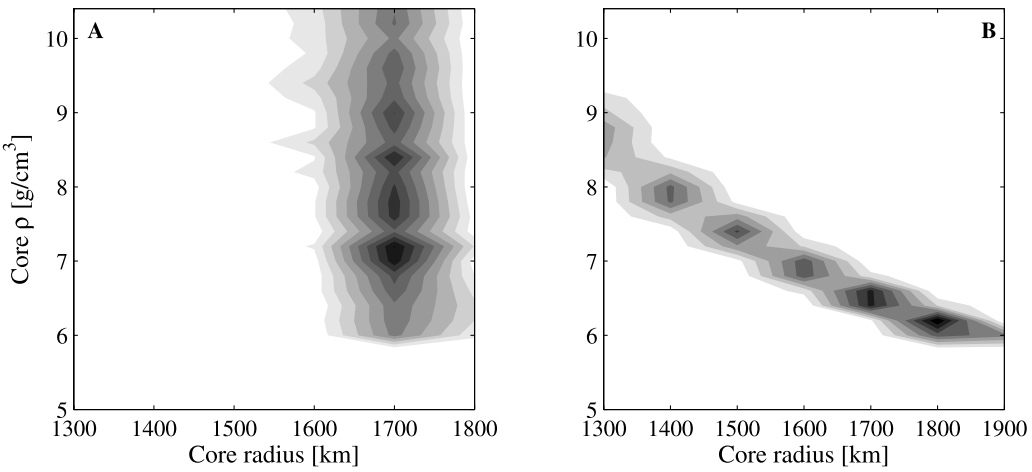

Figure 10. 2D marginal posterior *pdf*'s showing the correlation between sampled core densities and sizes for separate inversions of (a) k_2 and Q and (b) $\bar{\rho}$ and I . These plots indicate the sensitivity of subsets of the data to core properties. A significant narrowing in comparison to the prior *pdf* (Figure 8a) is obtained, implying that data are able to constrain these parameters. Shades of gray as before.

the inversion, i.e., ongoing from inversion of prior information (Figure 8a) over inversion of $\bar{\rho}$ and I, and inversion of k_2 and Q to inversion of all data (Figure 8b), the *pdf*'s narrow. This is further exemplified in the figures below, which in addition to the above also address issue of stationarity of the MCMC algorithm, i.e., similarity of inverted parameters across independent chains (using different random number sequences). Figure 11 below summarizes the results, in the form of sampled bulk Mg#s, for separate inversions of (1) prior information, (2) only k_2 and Q, (3) only $\bar{\rho}$ and I, and (4) joint inversion of all data, including results from an independent run. Sampled Mg#s from the two independent posterior chains vary in detail, but their overall characteristics are similar. As concerns inversion of individual data sets, we observe that while the characteristics are different to the full posterior *pdf*, separately inverted *pdf*'s are narrower than the prior *pdf*, implying that individual data sets are able to provide information on the system.

7. Conclusion

[65] We have applied a recently developed method to invert global geophysical data directly for composition and thermal state, rather than the physical property related to the particular geophysical field of interest. This bridges the inherent shortcoming of traditional methods seeking to infer the above parameters from geophysical field measurements, followed by interpretations based on laboratory results. We have shown that it is possible to obtain valuable information on the internal constitution of Mars from the set of presently available geophysical measurements. As emphasized it has not been the purpose to refine earlier results, but rather to investigate the range of models consistent with the geophysical observations. Previous results were mostly based on single forward modeling approaches and the DW-SNC model composition. In contrast, with our method we obtain a range of models that are consistent with data and derived independently of the model Martian mantle composition of DW. From these any measures of interest can be calculated, in addition to providing realistic estimates of error and resolution.

[66] Our results point to an FeO enriched Martian composition relative to the Earth, as also inferred from geochemical analyses of the SNC meteorites. Most other elements occur in proportions that are close to the Martian model composition derived from the SNC's. This is further

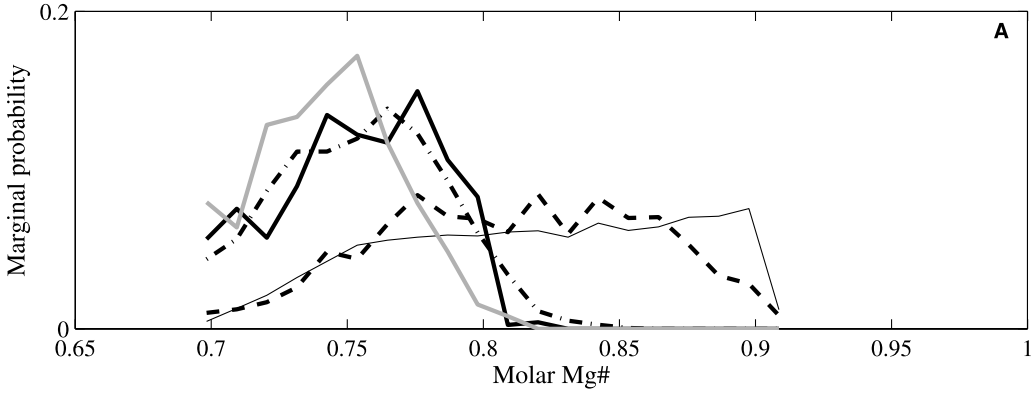

Figure 11. Marginal prior and posterior *pdf*'s showing sampled bulk silicate Mg#'s, obtained by inverting prior information (thin line), only $\bar{\rho}$ and I (dot-dashed line), only k_2 and Q (dashed line), all data jointly (heavy line), all data jointly with different random seed (gray heavy line), respectively.

indicated by the bulk silicate Mg# and Mg/Si ratios. Our mantle mineralogy generally encompasses the mineralogy found in previous studies, except for the absence, in our models, of a thin perovskite-bearing layer just above the CMB. Because its presence depended on the size and composition of the core, which could not be determined independently, most previous studies assumed perovskite to be stable, although the question remained open, inasmuch as core size could not be answered definitely. Concerning the latter, we found a core with a radius of around 1680 km, a density of $\sim$6.7 g/cm^3, and most probable CMB temperatures of $\sim$1800°C. Combining these results with recent laboratory measurements of melting relations in the Fe-FeS system and accompanying density measurements, we interpret our results, as implying a molten core, in concert with other recent findings, and containing $\sim$22–25 wt% S.

[67] On the basis of our results, we concur with earlier conclusions, which were based on more limited data then available, that it is not possible to fit the requirement of a bulk CI chondritic Fe/Si ratio with the available geophysical data. On the basis of these conclusions, the CI chondrite accretion model for Mars, and the terrestrial planets in general, probably needs to be reexamined. We propose that the building blocks might possibly be found among the ordinary chondrite groups L and LL, as their compositions concur with our estimates, and also match the oxygen isotopic composition of the SNC's.

[68] How can these results be refined in the future? The most obvious way is through the acquisition of geophysical data pertinent to its interior, in particular seismic data, in the form of traveltimes, surface waves, free oscillations or even noise [e.g., *Gudkova and Zharkov*, 2004; *Larose et al.*, 2005; *Khan et al.*, 2006a]. Seismology, because of its higher resolving power, in comparison to other geophysical techniques, holds the greatest potential of providing definite answers on the internal structure and constitution of planets. This obviously calls for a long overdue seismic mission to Mars.

[69] **Acknowledgments.** We would like to thank Oleg Kuskov, an anonymous reviewer and Francis Nimmo for comments that improved the manuscript. T. Gudkova kindly provided model M13. A. Khan acknowledges support from the Danish Agency for Science, Technology and Innovation.

References

Acuña, M. H., et al. (1999), Global distribution of crustal magnetization discovered by the Mars Global Surveyor MAG/ER experiment, *Science*, *284*, 790.

Agee, C. B., and D. S. Draper (2004), Experimental constraints on the origin of Martian meteorites and the composition of the Martian mantle, *Earth Planet. Sci. Lett.*, *224*, 415.

Alterman, Z., H. Jarosch, and C. L. Pekeris (1959), Oscillations of the Earth, *Proc. R. Soc., Ser A and Ser. B*, *A252*, 80.

Babeiko, A. Yu., and V. N. Zharkov (1997), Mineral composition and seismic model of the Martian crust, *Sol. Syst. Res.*, *31*, 361.

Belleguic, V., P. Lognonné, and M. Wieczorek (2005), Constraints on the Martian lithosphere from gravity and topography data, *J. Geophys. Res.*, *110*, E11005, doi:10.1029/2005JE002437.

Benjamin, D., J. Wahr, R. D. Ray, G. D. Egbert, and S. D. Desai (2006), Constraints on mantle anelasticity from geodetic observations, and implications for the J_2 anomaly, *Geophys. J. Int.*, *165*, 3.

Bertka, C., and Y. Fei (1997), Mineralogy of the Martian interior up to core-mantle boundary pressures, *J. Geophys. Res.*, *102*, 5251.

Bertka, C., and Y. Fei (1998a), Density profile of an SNC model Martian interior and the moment of inertia factor of Mars, *Earth Planet. Sci. Lett.*, *157*, 79.

Bertka, C., and Y. Fei (1998b), Implications of Mars Pathfinder data for the accretion history of the terrestrial planets, *Science*, *281*, 1838.

Bills, B. G., G. A. Neumann, D. E. Smith, and M. T. Zuber (2005), Improved estimate of tidal dissipation within Mars from MOLA observations of the shadow of Phobos, *J. Geophys. Res.*, *110*, E07004, doi:10.1029/2004JE002376.

Breuer, D., and T. Spohn (2003), Early plate tectonics versus single-plate tectonics on Mars: Evidence from magnetic field history and crust evolution, *J. Geophys. Res.*, *108*(E7), 5072, doi:10.1029/2002JE001999.

Burbine, T. H., and K. M. O'Brien (2004), Determining the possible building blocks of the Earth and Mars, *Meteorit. Planet. Sci.*, *39*, 667.

Chambers, J. E. (2001), Making more terrestrial planets, *Icarus*, *152*, 205.

Clayton, R. N., T. K. Mayeda, J. N. Goswami, and E. J. Olsen (1991), Oxygen isotope studies of ordinary chondrites, *Geochim. Cosmochim. Acta*, *55*, 2317.

Connerney, J. E. P., M. H. Acuña, P. J. Wasilevsky, N. F. Ness, H. Réme, C. Mallezem, D. Vignes, R. P. Lin, D. L. Mitchell, and P. A. Cloutier (1999), Magnetic lineations in the ancient crust of Mars, *Science*, *284*, 794.

Connolly, J. A. D. (2005), Computation of phase equilibria by linear programming: A tool for geodynamic modeling and an application to subduction zone decarbonation, *Earth Planet. Sci. Lett.*, *236*, 524.

Connolly, J. A. D., and D. M. Kerrick (2002), Metamorphic controls on seismic velocity of subducted oceanic crust at 100–250 km depth, *Earth Planet. Sci. Lett.*, *204*, 61.

Dreibus, G., and H. Wänke (1985), Mars: A volatile-rich planet, *Meteoritics*, *20*, 367.

Duffy, T. S., and D. L. Anderson (1989), Seismic velocities in mantle minerals and the mineralogy of the upper mantle, *J. Geophys. Res.*, *94*(B2), 1895–1912.

Elkins-Tanton, L. T., E. M. Parmentier, and P. C. Hess (2003), Magma ocean fractional crystallisation and cumulate overturn in terrestrial planets: Implications for Mars, *Meteorit. Planet. Sci.*, *38*, 1753.

Elkins-Tanton, L. T., P. C. Hess, and E. M. Parmentier (2005), Possible formation of ancient crust on Mars through magma ocean processes, *J. Geophys. Res.*, *110*, E12S01, doi:10.1029/2005JE002480.

Esposito, P. B., W. B. Banerdt, G. F. Lindal, W. L. Sjogren, M. A. Slade, B. G. Bills, D. E. Smith, and G. Balmino (1992), Gravity and topography, in *Mars*, edited by H. H. Kieffer et al., 209 pp., Univ. of Arizona Press, Tucson, Ariz.

Fabrichnaya, O. (1998), The assessment of thermodynamic parameters for solid phases in the Fe-Mg-O and Fe-Mg-Si-O systems, *Calphad.*, *22*, 85.

Fei, Y., and C. M. Bertka (2005), The interior of Mars, *Science*, *308*, 1120.

Fei, Y., L. Zhang, T. Komabayashi, N. Sata, and C. M. Bertka (2006), Evidences for a liquid Martian core, in *37th Lunar Planet. Sci. Conf.*, Abstract #1500.

Folkner, W. M., C. F. Yoder, D. N. Yuan, E. M. Standish, and R. A. Preston (1997), Interior structure and seasonal mass redistribution of Mars from radio tracking of Mars Pathfinder, *Science*, *278*, 1749.

Gudkova, T. V., and V. N. Zharkov (2004), Mars: Interior structure and excitation of free oscillations, *Phys. Earth Planet. Inter.*, *142*, 1.

Harder, H. (2000), Mantle convection and the dynamic geoid of Mars, *Geophys. Res. Lett.*, *27*, 301.

Hauck, S. A., and R. J. Phillips (2002), Thermal and crustal evolution of Mars, *J. Geophys. Res.*, *107*(E7), 5052, doi:10.1029/2001JE001801.

Hixson, R. S., M. A. Winkler, and M. L. Hodgon (2006), Sound speed and thermophysical properties of liquid iron and nickel, *Phys. Rev. B*, *42*, 6485.

Jackson, I., J. D. Fitz Gerald, U. H. Faul, and B. H. Tan (2002), Grain-size-sensitive seismic wave attenuation in polycrystalline olivine, *J. Geophys. Res.*, *107*(B12), 2360, doi:10.1029/2001JB001225.

Jarosewich, E. (1990), Chemical analyses of meteorites: A compilation of stony and iron meteorite analyses, *Meteoritics*, *25*, 323.

Kavner, A., T. S. Duffy, and G. Shen (2001), Phase stability and density of FeS at high pressure and temperatures: Implications for the interior structure of Mars, *Earth Planet. Sci. Lett.*, *185*, 25.

Khan, A., K. Mosegaard, J. G. Williams, and P. Lognonné (2004), Does the Moon possess a core? Probing the deep lunar interior using results from LLR and lunar prospector, *J. Geophys. Res.*, *109*, E09007, doi:10.1029/2004JE002294.

Khan, A., J. A. D. Connolly, J. Maclennan, and K. Mosegaard (2006a), Joint inversion of seismic and gravity data for lunar composition and thermal state, *Geophys. J. Int.*, *168*, 243, doi:10.1111/j.1365-246X.2006.03200.x.

Khan, A., J. A. D. Connolly, and N. Olsen (2006b), Constraining the composition and thermal state of the mantle beneath Europe from inversion of long-period electromagnetic sounding data, *J. Geophys. Res.*, *111*, B10102, doi:10.1029/2006JB004270.

Khan, A., J. A. D. Connolly, N. Olsen, and K. Mosegaard (2006c), Constraining the composition and thermal state of the Moon from an inver-

sion of electromagnetic lunar day-side transfer functions, *Earth Planet. Sci. Lett.*, *248*, doi:10.1016/j_enh.epsl.2006.04.008.
Konopliv, A. S., C. F. Yoder, E. M. Standish, D. Yuan, and W. L. Sjogren (2006), A global solution for the Mars static and seasonal gravity, Mars orientation, Phobos and Deimos masses, and Mars ephemeris, *Icarus*, *182*, 23.
Kuskov, O. L., and A. B. Panferov (1993), Thermodynamic models for the structure of the Martian upper mantle, *Geochem. Int.*, *30*, 132.
Kuskov, O. L., and V. A. Kronrod (2001), L- and LL-chondritic models of the chemical composition of Io, *Sol. Syst. Res.*, *35*, 218.
Kuskov, O. L., and V. A. Kronrod (2005), Internal structure of Europa and Callisto, *Icarus*, *177*, 550.
Kuskov, O. L., V. A. Kronrod, and L. L. Hood (2002), Geochemical constraints on the seismic properties of the lunar mantle, *Phys. Earth Planet. Int.*, *134*, 175.
Lainey, V., V. Dehant, and M. Patzold (2007), First numerical ephemerides of the Martian moons, *Astron. Astrophys.*, *465*, 1075.
Larose, E., A. Khan, Y. Nakamura, and M. Campillo (2005), Lunar subsurface investigated from correlation of seismic noise, *Geophys. Res. Lett.*, *32*, L16201, doi:10.1029/2005GL023518.
Lodders, K., and B. Fegley (1997), An oxygen isotope model for the composition of Mars, *Icarus*, *126*, 373.
Lognonné, P., and B. Mosser (2003), Planetary seismology, *Surv. Geophys.*, *14*, 239.
Longhi, J., E. Knittle, J. R. Holloway, and H. Wänke (1992), The bulk composition, mineralogy and internal structure of Mars, in *Mars*, edited by H. H. Kieffer et al., 184 pp., Univ. of Arizona Press, Tucson, Ariz.
McDonough, W. F., and S. S. Sun (1995), The composition of the Earth, *Chem. Geol.*, *120*, 223.
McSween, H. Y. (1994), What have we learned about Mars from SNC meteorites, *Meteoritics*, *29*, 757.
Mosegaard, K. (1998), Resolution analysis of general inverse problems through inverse Monte Carlo sampling, *Inverse Probl.*, *14*, 405.
Mosegaard, K., and A. Tarantola (1995), Monte Carlo sampling of solutions to inverse problems, *J. Geophys. Res.*, *100*, 12,431.
Neumann, G. A., M. T. Zuber, M. A. Wieczorek, P. J. McGovern, F. G. Lemoine, and D. E. Smith (2004), Crustal structure of Mars from gravity and topography, *J. Geophys. Res.*, *109*, E08002, doi:10.1029/2004JE002262.
Sanloup, C., A. Jambon, and P. Gillet (1999), A simple chondritic model of Mars, *Phys. Earth Planet. Int.*, *112*, 43.
Schubert, G., C. T. Russell, and W. B. Moore (2000), Timing of the Martian dynamo, *Nature*, *408*, 666.
Segatz, M., T. Spohn, M. N. Ross, and G. Schubert (1988), Tidal dissipation, surface heat flow, and figure of viscoelastic models of Io, *Icarus*, *75*, 187.
Smith, D. E., M. T. Zuber, M. H. Torrence, and P. J. Sunn (2003), Estimating the k_2 tidal gravity Love number of Mars, *Eos. Trans. AGU*, *84*(46), Fall. Meet. Suppl., abstract P31A-05.
Sohl, F., and T. Spohn (1997), The interior structure of Mars: Implications from SNC meteorites, *J. Geophys. Res.*, *102*, 1613.
Sohl, F., G. Schubert, and T. Spohn (2005), Geophysical constraints on the composition and structure of the Martian interior, *J. Geophys. Res.*, *110*, E12008, doi:10.1029/2005JE002520.
Solomon, S. C., et al. (2005), New perspectives on ancient Mars, *Science*, *307*, 1214.
Stevenson, D. J. (2001), Mars' core and magnetism, *Nature*, *412*, 214.
Stewart, A. J., M. W. Schmidt, W. van Westrenen, and C. Liebske (2007), Mars: A new core-crystallisation regime, *Science*, *316*, 13.
Stixrude, L., and C. Lithgow-Bertelloni (2005), Mineralogy and elasticity of the oceanic upper mantle: Origin of the low-velocity zone, *J. Geophys. Res.*, *110*, B03204, doi:10.1029/2004JB002965.
Stixrude, L., and M. S. T. Bukowinski (1990), Fundamental thermodynamic relations and silicate melting with implications for the constitution of D″, *J. Geophys. Res.*, *95*, 19,311.
Tarantola, A., and B. Valette (1982), Inverse problems: Quest for information, *J. Geophys.*, *50*, 159.
Taylor, S. R. (1999), On the difficulty of making Earth-like planets, *Meteorit. Planet. Sci.*, *34*, 317.
Treiman, A. H. (1986), The parental magma of the Nakhla achondrite: Ultrabasic volcanism on the shergottite parent body, *Geochim. Cosmochim. Acta*, *50*, 1061.
Van Thienen, P., A. Rivoldini, T. van Hoolst, and P. Lognonné (2006), A top-down origin for Martian mantle plumes, *Icarus*, *185*, 197, doi:10.1016/j.icarus.2006.06.08.
Verhoeven, O., et al. (2005), Interior structure of terrestrial planets: Modeling Mars' mantle and its electromagnetic, geodetic, and seismic properties, *J. Geophys. Res.*, *110*, E04009, doi:10.1029/2004JE002271.
Wahr, J. M., and Z. Bergen (1986), The effects of mantle elasticity on nutations, Earth tides and tidal variation in rotation rate, *Geophys. J. R. Astron. Soc.*, *87*, 633.
Wasson, J. T., and G. W. Kallemeyn (1988), Compositions of chondrites, *Philos. Trans. R. Soc. London Ser. A*, *325*, 535.
Weiss, B. P., H. Vali, F. J. Baudenbacher, J. L. Kirschvink, S. T. Stewart, and D. L. Shuster (2002), Records of an ancient Martian magnetic field in ALH84001, *Earth Planet. Sci. Lett.*, *201*, 449.
Wetherill, G. W. (1994), Provenance of the terrestrial planets, *Geochim. Cosmochim. Acta*, *58*, 4513.
Wieczorek, M. A., and M. T. Zuber (2004), Thickness of the Martian crust: Improved constraints from geoid-to-topography ratios, *J. Geophys. Res.*, *109*, E01009, doi:10.1029/2003JE002153.
Williams, J. P., and F. Nimmo (2004), Thermal evolution of the Martian core: Implications for an early dynamo, *Geology*, *32*, 97.
Wood, B. J., and J. R. Holloway (1984), A thermodynamic model for subsolidus equilibria in the system CaO-MgO-Al2O3-SiO2, *Geochim. Cosmochim. Acta*, *66*, 159.
Yoder, C. F. (1982), Tidal rigidity of Phobos, *Icarus*, *49*, 327.
Yoder, C. F., A. S. Konopliv, D. N. Yuan, E. M. Standish, and W. M. Folkner (2003), Fluid core size of Mars from detection of the solar tide, *Science*, *300*, 299.
Zharkov, V. N. (1996), The internal structure of Mars: A key to understanding the origin of terrestrial planets, *Sol. Syst. Res.*, *30*, 456.
Zharkov, V. N., and T. V. Gudkova (1997), On the dissipative factor of the Martian interiors, *Planet. Space Sci.*, *45*, 407.
Zharkov, V. N., and T. V. Gudkova (2005), Construction of Martian interior model, *Solar Syst. Res.*, *39*, 387.
Zschau, J. (1978), Tidal friction in the solid Earth: Loading tides versus body tides, in *Tidal Friction and the Earth's Rotation*, edited by P. Brosche and J. Sundermann, 62 pp., Springer, New York.
Zuber, M. T. (2001), The crust and mantle of Mars, *Nature*, *412*, 220.

J. A. D. Connolly, Earth Sciences Department, Swiss Federal Institute of Technology, Clausiusstr. 25, 8092 Zurich, Switzerland. (james.connolly@erdw.ethz.ch)
A. Khan, Niels Bohr Institute, University of Copenhagen, Juliane Maries Vej 30, 2100 Copenhagen Oe, Denmark. (amir@gfy.ku.dk)